REPORT DOCUMENTATION PAGE

AFRL-SR-BL-TR-98-

0260

1. AGENCY USE ONLY (Leave blank)	2. REPORT DATE	3. REPORT TYPE AND DATES COVERED
	February 1998	Final Report 7/1/96 - 10/31/97

4. TITLE AND SUBTITLE
Effects of Strain Rate and Moisture on the Tensile Strength of Heterogeneous Materials

5. FUNDING NUMBERS
F49620-96-1-0333

6. AUTHOR(S)
C. A. Ross

7. PERFORMING ORGANIZATION NAME(S) AND ADDRESS(ES)
University of Florida
Graduate Engineering and Research Center
1350 No. Poquito Road
Shalimar, FL 32579

8. PERFORMING ORGANIZATION REPORT NUMBER

9. SPONSORING/MONITORING AGENCY NAME(S) AND ADDRESS(ES)
Air Force Office of Scientific Research
Aerospace & Materials Sciences
AFOSR/NA
110 Duncan Ave., Suite B115
Bolling AFB, DC 20332-0001

NA

10. SPONSORING/MONITORING AGENCY REPORT NUMBER

11. SUPPLEMENTARY NOTES

12a. DISTRIBUTION/AVAILABILITY STATEMENT
Approved for public release
Distribution unlimited

12b. DISTRIBUTION CODE

13. ABSTRACT *(Maximum 200 words)*

Strain rate effects on tensile strength of concrete and mortar were investigated using three different size specimens, two different sized split Hopkinson pressure bars (SHPB) and a standard material test machine. All combinations of data show the same trend of abrupt increases in tensile strength at a strain rate of about 1.0/sec. An analytical expression and an empirical relation for concrete tensile strength are presented as functions of strain rate and crack velocity. Crack velocity of concrete and mortar as a function of strain rate was determined using ultra high-speed photography, crack gages, and time of failure for splitting tensile tests in a SHPB. Crack velocity data shows an asymptotic tendency toward the limiting crack velocity, at a strain rate between 20 - 70/sec. Fracture toughness, at quasistatic strain rates for concrete and mortar are presented. A malfunction on the ultra high-speed camera prevented the completion of fracture toughness data at high strain rates. Dynamic precompression pulses applied to SHPB specimens were used to show that crack damage results in tensile strength reductions in concrete and mortar. Ultrasonic wave velocity measurements of the damaged specimens showed damage is directional and should not be treated as a simple scaler.

14. SUBJECT TERMS	15. NUMBER OF PAGES
Concrete, Mortar, Rate Effects, Damage, Crack Velocity, Failure, Fracture, Fracture Toughness	46
	16. PRICE CODE

17. SECURITY CLASSIFICATION OF REPORT	18. SECURITY CLASSIFICATION OF THIS PAGE	19. SECURITY CLASSIFICATION OF ABSTRACT	20. LIMITATION OF ABSTRACT
unclassified	unclassified	unclassified	

TABLE OF CONTENTS

LIST OF FIGURES

Figure

LIST OF TABLES

Table

I. EXECUTIVE SUMMARY

1. Objective

The major objective of this study is to examine the effects of strain rate and moisture on the tensile strength of heterogeneous materials such as concrete and mortar.

2. Background

Effects of increasing strain rate on the tensile strength of concrete has been recognized for several years and experimental data indicates a gradual increase in tensile strength of approximately 50 percent from a quasistatic strain rate of 1×10^{-6}/sec to 1.0 sec. After 1.0/sec a considerable increase as much as seven times the quasistatic strength, occurs at strain rates of 10 to 20/sec.

Direct tension test of concrete or mortar is very difficult even at quasistatic strain rates. Therefore, a splitting tensile test (Brazilian) is employed in a split Hopkinson pressure bar (SHPB) for high strain rates and a standard material test machine is used at low strain rates. Effects of strain rate on the tensile strength of concrete are different for various mixes with different concrete compressive strength. The compressive twenty-eight day cylinder strength is the standard by which concrete strength is compared. Concrete having lower compressive strength show increased strain rate sensitivity at strain rates lower than that of higher strength concrete. This is viewed as increased strain rate sensitivity for the lower strength material because the lower strength concrete shows a higher percentage of strength increase, for a given strain rate, than that of the higher strength material. Since water saturated concrete shows a decrease in compressive strength when compared to the same dry concrete, it is expected to show increased strain rate sensitivity at high strain rates over that of the same dry material.

Both dry and saturated concrete are expected to show increased concrete fracture toughness and increased crack velocity when tested at high strain rates. Notched and unnotched splitting tensile specimens will be tested both at low and high strain rates to examine the strain rate effects.

3. Scope

The general approach in this study is to measure tensile strength, crack velocity and strain rate of concrete and mortar specimens subjected to low strain rate in a standard material test machine and high rates in a SHPB.

4. Methodology

Concrete and mortar specimens will be cast in several size cylindrical molds, cured and cut to size for testing. Both notched and unnotched specimens will be tested to failure using a standard material test machine and two different sized split Hopkinson pressure bars (SHPB). Ultra high-speed photography capable of a million frames per second will be used to study the dynamic fracture process. Crack gages will be placed on some specimens to measure crack velocity in conjunction with the high-speed photography. Dynamic precompression pulses will be applied to some specimens then subsequently tested by ultrasonics to measure stress wave velocities before and after precompression. After wave velocity measurements the precompressed specimens will be tested to failure by dynamic tensile tests.

Crack velocity and fracture toughness data will be used in determining analytical expressions of tensile strength at high strain rates.

5. Results

Both high and low strain tensile strength data were obtained for concrete and mortar using three different size specimens in two different size SHPB's. All the strength show similar trends

which compare well with other data found in the literature. Analytical and empirical equations for tensile strength as a function of strain rate are presented.

Crack velocity data when plotted versus strain rate show an asymptotic approach to a limiting velocity based on forty to sixty percent of the bar velocity of the material.

Results of dynamic precompression tests showed that damage due to cracking should be treated as directional and not a simple scaler.

Work on material fracture parameters was accomplished on notched specimens and the analysis was inconclusive. Additional hole notched specimens were fabricated to increase the notch sensitivity. However, the high-speed camera malfunctioned just as we were to test these specimens. This occurred just prior to the end of our grant period and the camera was down for over three months. As a result of the camera the material fracture parameters could not be included in this report.

6. Conclusions

Concrete tensile strength collected for several test methods show the same trends, indicating a gradual rise in concrete tensile strength up to a strain rate of approximately 1.0/sec followed by a seven-fold increase in strength up to an approximate 20/sec strain rate.

Crack velocity data shows an increase of crack velocity with strain rate and appears to asymptotically approach the limiting crack velocity at a strain rate between 20/sec and 70/sec depending on the value of the limiting velocity.

Based on crack damage and ultrasonic wave velocity measurement, the damage parameter should be treated as directional and not a simple scaler. Reduction of ultrasonic wave velocity of approximately thirty percent is an indication of severe damage.

II. EXPERIMENTAL INVESTIGATION

1. Introduction

In order to characterize concrete and mortar for some basic quasistatic and dynamic mechanical properties both a standard material test machine (SMTM) and a split Hopkinson pressure bar (SHPB) were used. A SMTM uses a mechanical or hydraulic system to apply pressure to a specimen and is equipped with load cells and displacement measuring devices to quantify load, load rate, displacement and displacement rate applied to the specimen. The usual SMTM for concrete testing is capable of applying loads at a rate of a few kPa per minute up to several MPa/min. For concrete the tensile loading rate, in the quasistatic range, recommended by ASTM C496, is 100 to 200 psi/min (0.69 to 1.38 MPa/min). For concrete with a Young's modulus of 20 to 40 GPa (3 to 6 Mpsi) this results in a strain rate of 3 to 7 microstrains/sec.

A typical SHBP, when testing metals, may produce strain rates on the order of 1 to 1000/sec due to the ability to use small specimen sizes. However, when testing concrete a larger specimen size is necessary if a large aggregate to sand grain size is desired. For these conditions the resulting tensile strain rate is reported to be on the order of 0.1 to 20/sec [1]. A typical concrete SHPB specimen recommended by Ross [1] and Malvern and Ross [2] should be no smaller than 50.4mm in diameter with five to ten aggregates across the diameter and along the length of the specimen. A reasonable aggregate size is on the order of five to ten millimeters. A review of the operation of the SHPB is given in the next section.

2. Split Hopkinson Pressure Bar (SHPB)

The split Hopkinson pressure bar operation was developed by Kolsky [3] and based on a modification of a conventional pressure bar used by Hopkinson [4]. The principles of operation of the SHPB are given in some detail by Nicholas [5]. Applications of the SHPB for concrete are

described in Kormeling et al. [6] and Malvern and Ross [2] and the use of the splitting tensile or Brazilian test is described by Ross [1].

Dynamic testing using the SHPB is based on a stress wave induced in a metal incident rod (usually cylindrical) by impact of a striker bar, usually of the same diameter and material as the incident bar. Using the schematic of Figure 1a, the stress wave travels down the incident bar, impinges on the specimen sandwiched between the incident bar and the transmitter bar and is partially reflected and transmitted into the incident and transmitter bars, respectively. Strain gages placed on the bars as shown in Figure 1a record the strain pulse of the stress waves in the two bars. For the compression mode of Figure 1b a cylindrical concrete specimen of length to diameter of unity is placed in series with the bars and it may be shown [5] that the strain in the specimen is proportional to the integral of the reflected strain pulse and the stress in the specimen is proportional to the transmitted strain pulse. Using this data a dynamic compressive stress-strain diagram may be drawn.

Dynamic tensile tests of concrete using a direct tensile specimen requires a similar SHPB device as that of Figure 1 except that a tensile stress wave must be induced by a striker sliding on the incident bar fitted with a tup. This type device is described in References [1] and [6] but has several drawbacks i.e., the specimen must be cemented in place, failure will occur at random sites in the specimen unless a reduced section is used and the induced tensile wave using a sliding striker and a tup has a much longer rise time than the conventional compressive pulse of a colinear of impact of bars.

In an effort to alleviate the difficulties of the direct tension test of concrete, Ross [1] experimented with the splitting tensile arrangement of Figure 1c. For this test the same size specimen as the compressive specimen is placed in a transverse position and loaded by use of

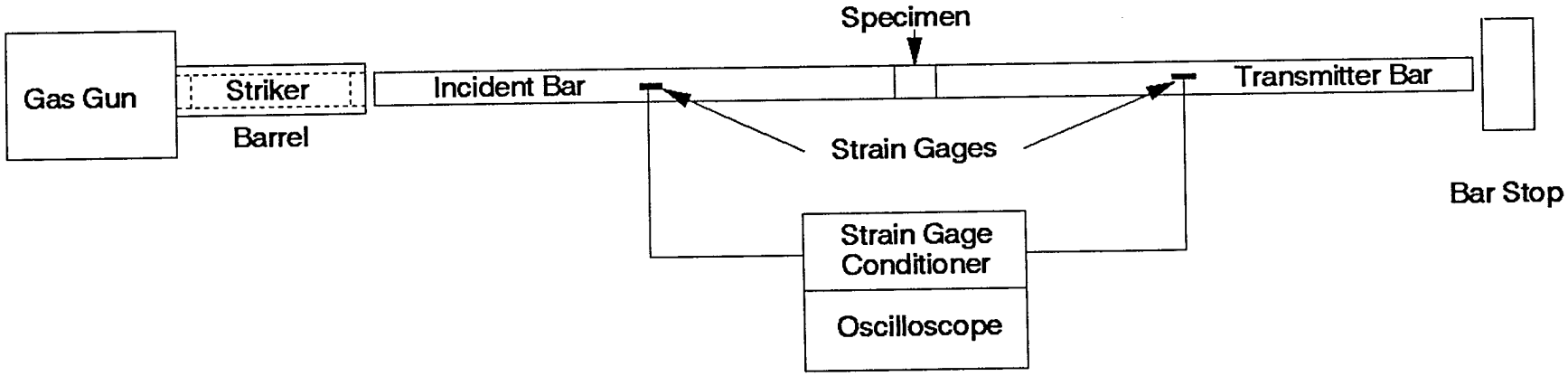

a) Split Hopkinson Pressure Bar (SHPB)

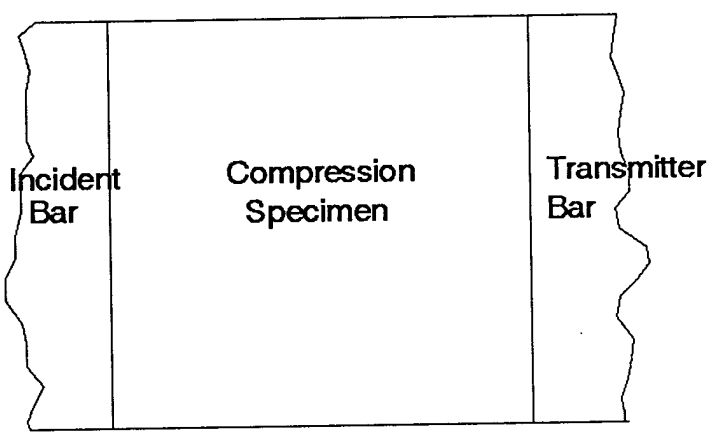

b) Specimen Arrangement for Compression Test

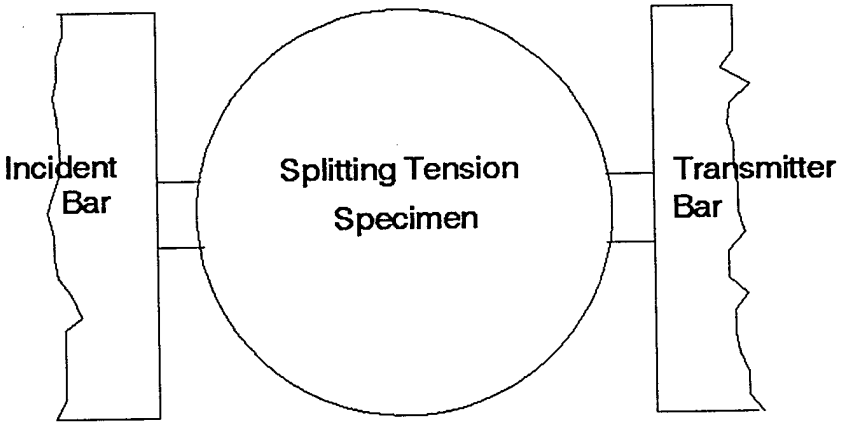

c) Specimen Arrangement for Splitting Tension Test

Figure 1. Schematic of a split Hopkinson pressure bar (SHPB) showing an arrangement for the compressive and splitting tensile specimens.

metal loading strips as shown in Figure 1c. For quasistatic tests, wooden loading strips are recommended but in the SHPB too much energy of the loading pulse is required to deform the wooden strips.

The one disadvantage of the splitting tensile test in the SHPB is that the specimen is not a true SHPB specimen and the use of the reflected strain pulse to obtain the specimen strain is not correct. However, it is assumed that the transmitted strain pulse is proportional to the load in the specimen. In addition a finite element analysis of the concrete splitting tensile specimen by Tedesco et al. [7] does verify a reasonable uniformity of tensile stress, along the specimen diameter parallel to the loading, at failure of the specimen. Based on these assumptions analyses of the tensile strength and strain rate of the splitting tensile concrete are given below.

3. Analysis Of The Concrete Splitting Tensile Test In The SHPB

The elastic solution of the splitting tensile test may be determined using equations and principles given in any elasticity text such as Timoshenko and Goodier [8]. The resulting equation given by Neville [9] predicts the tensile stress σ_t along the specimen diameter parallel to the loads as,

$$\sigma_t = \frac{2P}{\pi LD} \tag{1}$$

where P = applied load

L = specimen length

D = specimen diameter.

The tensile stress σ_t is constant over approximately eighty percent of the specimen diameter and the remainder of the diameter at the outer edge under the load is in compression. Specimen failure under both static and dynamic loadings exhibits very similar failure as shown in Figure 2a.

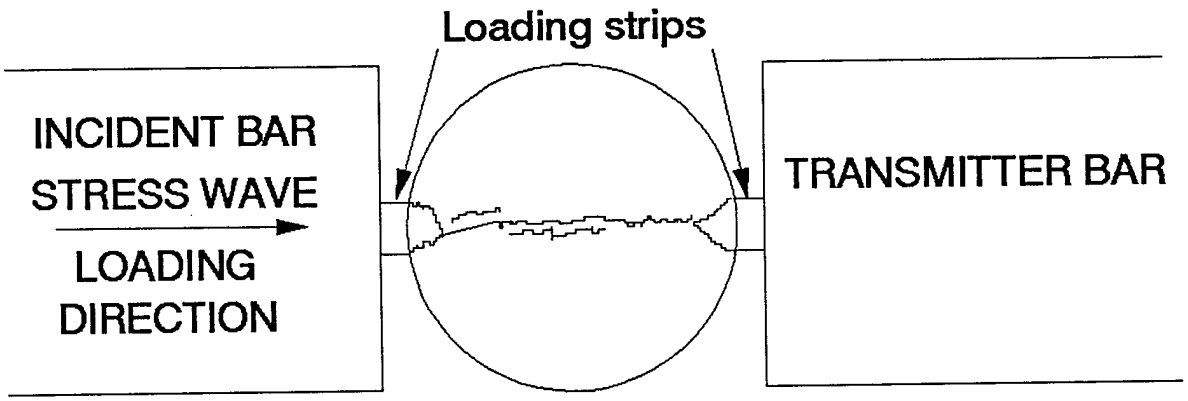

a) SPLITTING TENSILE SPECIMEN

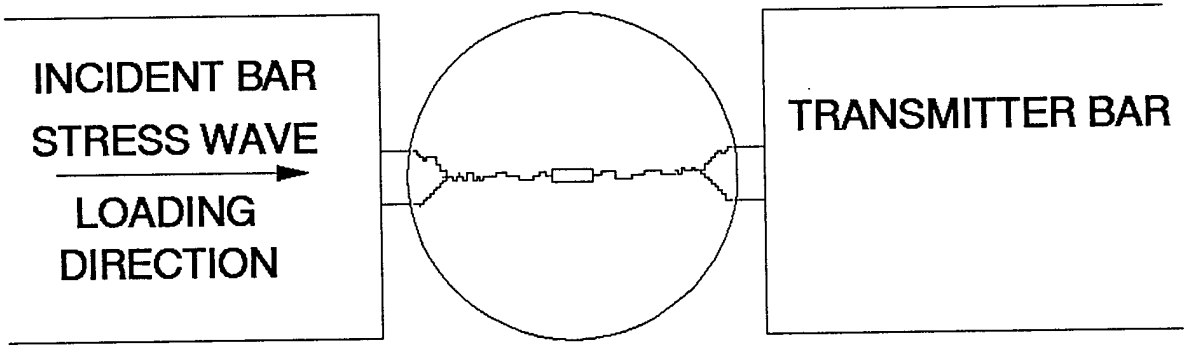

b) NOTCHED SPLITTING TENSILE SPECIMEN

Figure 2. Unnotched and notched splitting tensile specimens in a SHPB.

Compressive stresses at the edges, under the loading, produce the small triangular fractured pieces of the specimens.

It is assumed that the load P of Equation (1) may be determined from the strain pulse of the transmitted signal of the transmitter bar. Since the bars remain elastic the stress σ_t in the transmitter bar is

$$\sigma_T = \varepsilon_T E_b \tag{2}$$

where ε_T is the transmitted strain and E_b is the bar modulus. Using σ_T and the area of the bar the tensile stress becomes

$$\sigma_t = \frac{2R_b^2 \sigma_T}{LD} \tag{3}$$

where R_b is the bar radius. Figure 3 shows a transmitted stress curve with strength or peak stress and time to failure as noted. The average strain rate of the specimen is taken as the slope of the linear portion of the stress time curve, as shown in Figure 3, divided by the quasistatic modulus of the concrete. A general expression for the tensile strain rate $\dot{\varepsilon}_t$ is given as

$$\dot{\varepsilon}_t = \frac{\Delta\sigma_t}{E_C(\Delta t)} \tag{4}$$

where $\Delta\sigma_t$ is the change in stress, Δt is the change in time, and E_C is the modulus of the concrete. In cases where the modulus was not measured the general ACI equation [10] given as Equation (5) below was used

$$\left.\begin{aligned} E_c &= 57000\sqrt{f_c^1} \\ E_c &= 4734\sqrt{f_c^1} \end{aligned}\right\} \tag{5}$$

where f_c^1 is the twenty-eight day compressive strength given in the first equation as psi and given in the second equation as MPa.

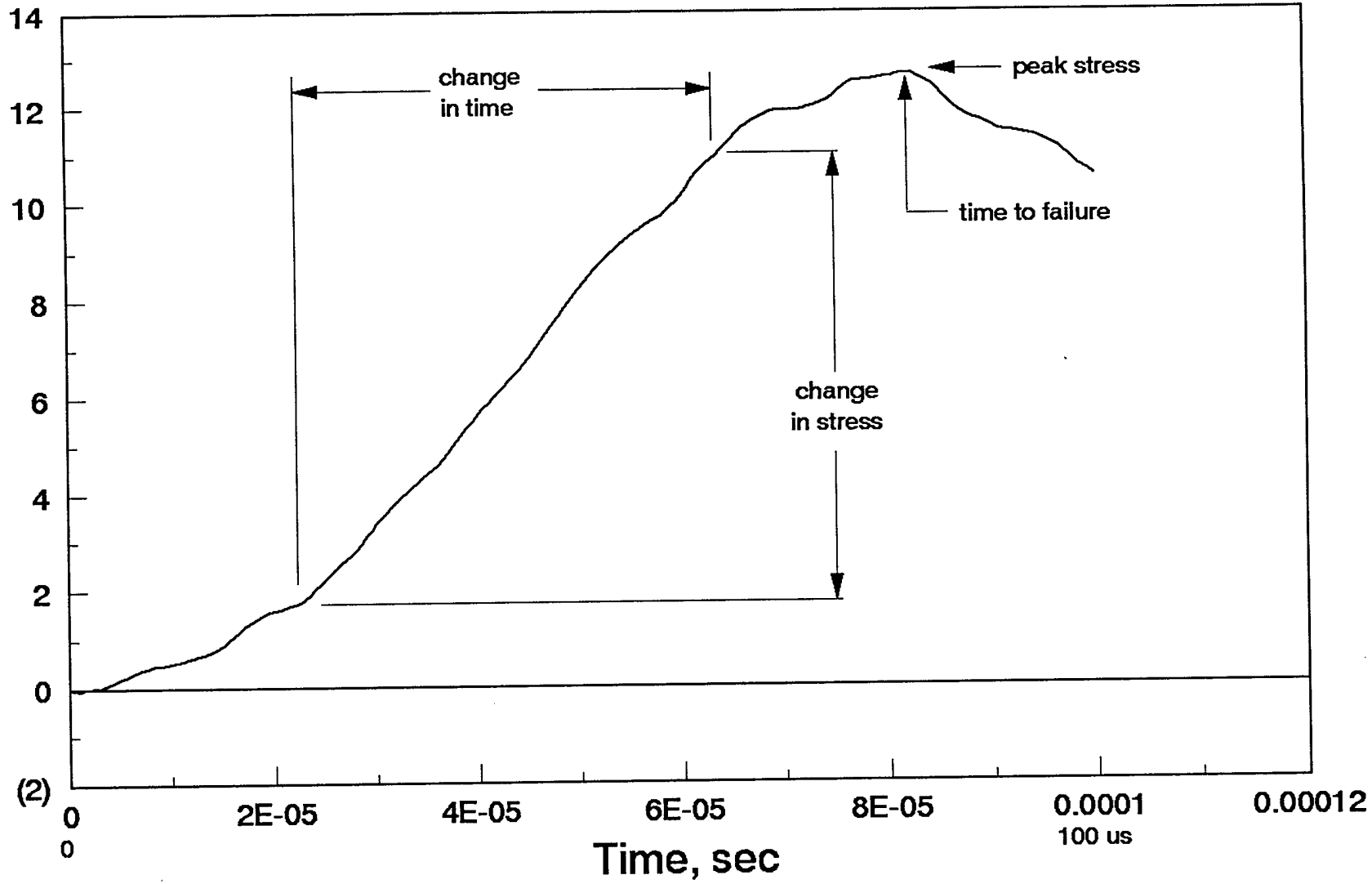

Figure 3. Transmitted stress-time signal from splitting tensile specimen in SHPB.

4. Crack Velocity Measurement

Crack velocity measurement was attempted using three different methods. In all methods a notched cylindrical specimen was used, as shown schematically in Figure 2b and Figure 4. This notched specimen is based on an extensive analysis and database compiled by Tang [11] and Tang et al. [12] in establishing a fracture toughness specimen. Various size notches were cast in 50.8mm and 76.2mm diameter concrete and mortar cylindrical specimens using thin stainless blades aligned with the central axis. The blades were angled on each edge to produce a pointed notch and were extracted approximately twenty-four hours after casting.

Crack velocity measurements were made using a thin foil resistive gages called KRAK gages manufactured by TTI Division, Hartrun Corp. of St. Augustine, FL in conjunction with an ultra-high speed digital camera (Imacon 468, Hadland Corp. UK). A KRAK gage is shown mounted on the specimen in a quasistatic test and a dynamic test of Figure 5.

The KRAK gage produces an electrical signal which is proportional to crack length when displayed versus time. Average crack velocity of the specimen is determined by the slope of this crack length versus time. In addition, a second method of crack velocity is used by observing the crack motion in the displayed frames from the high-speed camera. Exposure time of the camera was maintained at eighty nanoseconds and eight exposures were obtained at five microsecond intervals.

The third method for approximating the crack velocity is to use the time to failure, shown in Figure 3, and the distance the crack travels from the notch tip to the edge of the tensile stress domain. As shown in Figure 4 the tensile stress domain extends to approximately eighty percent of the specimen radius.

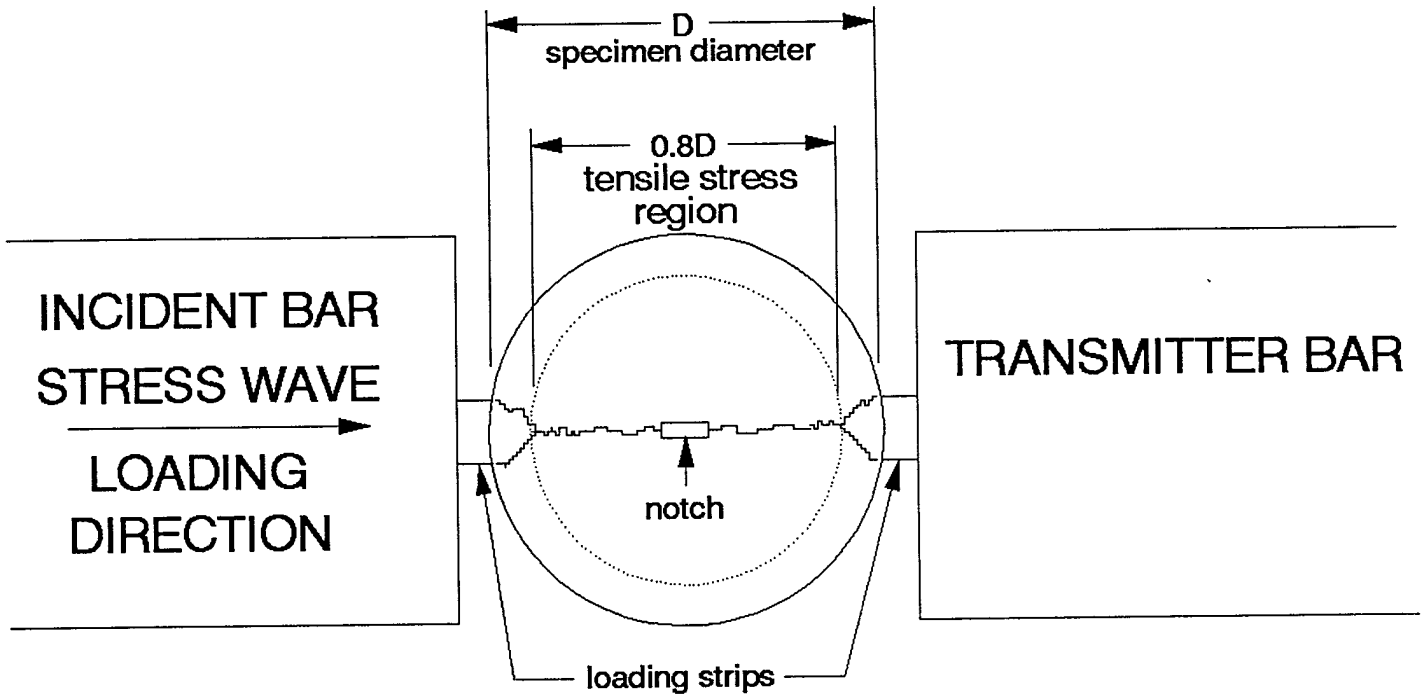

Figure 4. Notched splitting tensile specimen showing the extent of the fractured regions.

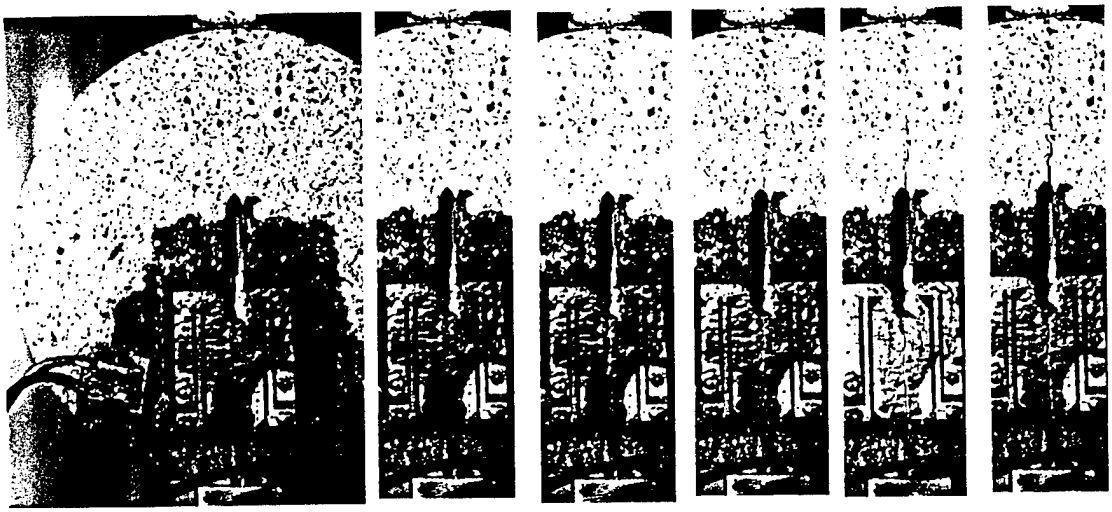

a) quasistatic

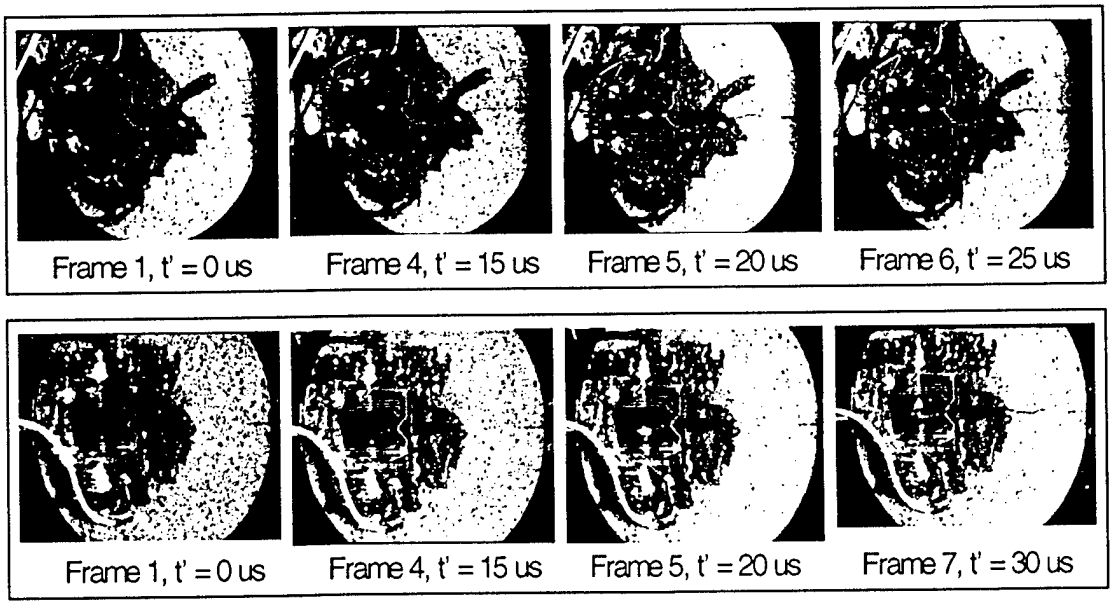

b) dynamic (two tests)

Figure 5. Photographs of the KRAK gage in place showing the crack progressing through the gage and specimen.

In all dynamic crack velocity measurement specimens the SHPB transmitted stress versus time (Figure 3) traces were recorded and strain rate as described earlier was calculated for each crack velocity measurement. In general, as will be shown in later sections, these three collection methods produced complimentary results. For quasistatic tests, crack velocity measurements were taken using the KRAK gage method of data collection.

5. Effects Of Dynamic Precompression On Dynamic Tensile Strength

In an effort to determine the effect of dynamic precompression on the dynamic tensile strength a series of mortar specimens were subjected to varying magnitude compressive stress waves using the compression mode (Figure 1b) of the SHPB. Preliminary testing was done to determine at what level of incident pressure was required to produce visible crack damage on the outside of the specimen. Any level above this critical incident pressure will cause break up of the specimen. After this critical incident pressure was determined, a series of specimens were subjected to incident pressures varying in five increments of the critical incident pressure.

After the precompression load several specimens were tested to failure at a fixed tensile strain rate. The splitting tensile test was used to determine the tensile strength of each of the precompressed specimens. The constant strain rate for the tests was determined in the earlier splitting tensile tests of solid unnotched cylinders. In addition, stress wave velocities, in both longitudinal and transverse directions of the specimens, were determined using ultrasonic methods. Transverse measurements of the cylinders were obtained after parallel flat surfaces were sawed on some of the precompressed cylinders. The ultrasonic device used was a C. N. S. Electronics "Portable Ultrasonic Non-Destructive Digital Indicating Tester," with a 150 kHz transducer set.

III. RESULTS AND DISCUSSION

1. Specimen Fabrication and Properties

Both concrete specimens, using limestone aggregate and sand, and mortar using only sand were cast in 2 inch diameter (50.8mm), 3 inch diameter (76.2mm) and 4 inch diameter (101.6mm) standard ASTM molds for use in the SHPB tests. For static properties characterization cylinders of 4" diameter x 8" long (10.16cm x 20.32cm) were also cast. Mix proportions for the concrete and mortar are given in Table 1 and the sieve analysis for concrete aggregate and sand are given in Figure 6.

Table 1
Mix Proportions for Concrete and Mortar

Concrete	Mortar
Portland Cement 270g	Portland Cement 450g
Limestone, Sieve #3/8-4 1242g	Sand, Sieve #4 1620g
Sand, Sieve #4 972 g	WRDA-19, 0.5% 3.7g
"F" Fly Ash 178.2g	"F" Fly Ash 297g
Water, w/c = 0.6 270g	Water, w/c = 0.55 411g

Quasistatic properties of both concrete and mortar at twenty-eight days are given in Table 2.

Table 2
Quasistatic Properties of Concrete and Mortar

1. Concrete, 28 Day Tests, 4"D x 8"L	
a) Compressive Strength	5012 psi (34.57 MPa)
Approximate Strain Rate	6.7×10^{-6}/sec
Modulus, $57000\sqrt{f_c'}$	4.03×10^{6} psi (27.8 GPa)
b) Tensile Strength (Sp. Ten.)	446 psi (3.08 MPa)
Approximate Strain Rate	3.6×10^{-7}/sec
2. Mortar, 28 Day Tests, 4"D x 8"L	
a) Compressive Strength	6116 psi (42.18 MPa)
Approximate Strain Rate	5.9×10^{-6}/sec
Modulus, $57000\sqrt{f_c'}$	4.46×10^{6} psi (30.8 GPa)
b) Tensile Strength (Sp. Ten.)	426 psi (2.94 MPa)
Approximate Strain Rate	3.76×10^{-7}/sec

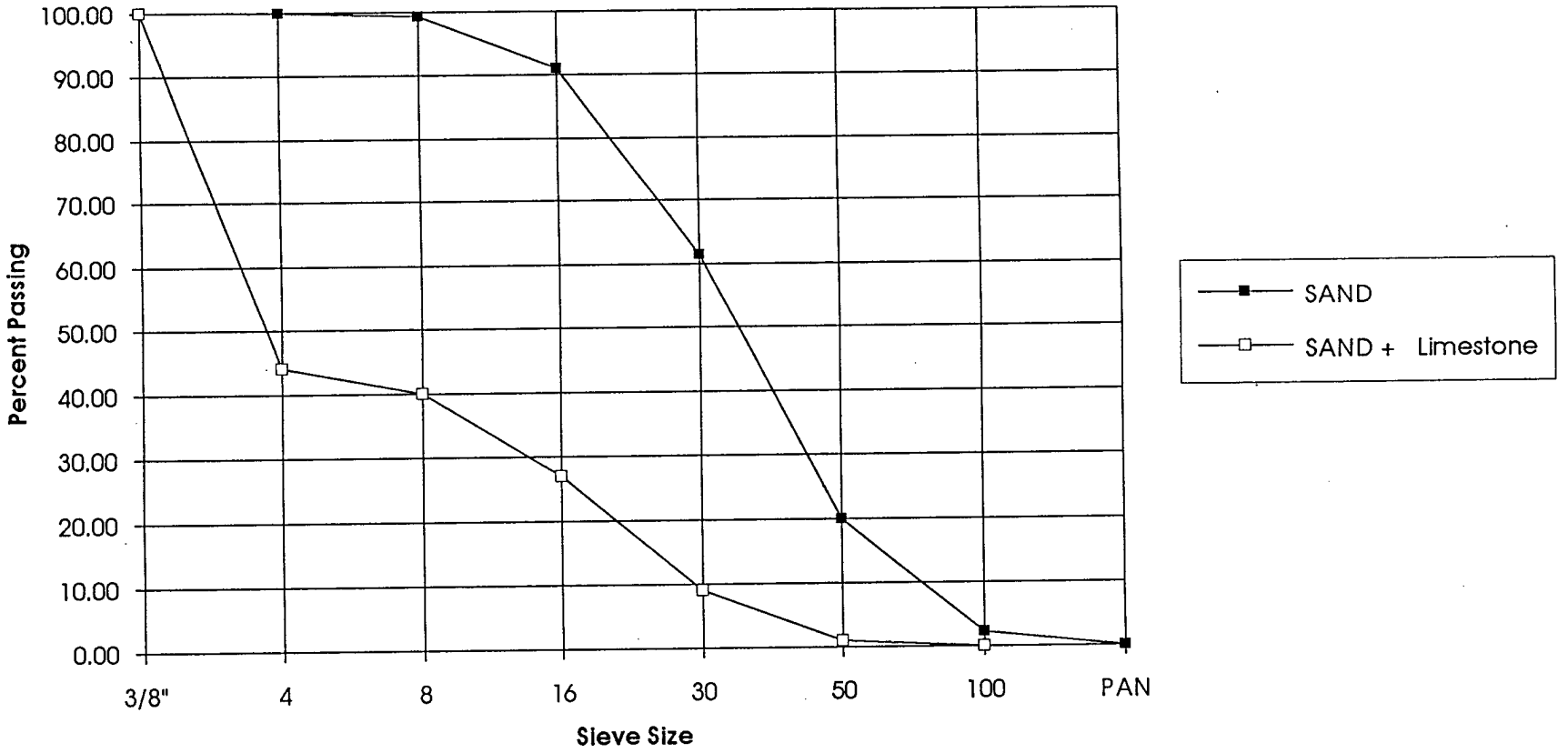

Figure 6. Sieve analysis of sand used in mortar mix and sand plus limestone aggregate used in concrete mix.

The quasistatic properties of the smaller specimens are required for the normalization of the SHPB tests. Quasistatic tests were performed again on the concrete and mortar at the time of the SHPB dynamic tests. In addition to quasistatic tests on the 4"D x 8"L (10.16 x 20.32cm) cylinders, compressive and splitting tensile tests were performed on the smaller diameter specimens using the same method of loading as to be encountered in the SHPB tests. This data is given in Table 3.

Similar compressive strengths for the two mixes was desired, the test results proved differently and recasting of a different mix was not a viable option, so the specimens were used as casts. Equation (5) was used to determine the modulus of the concrete and mortar.

Table 3
Quasistatic Concrete and Mortar Properties
at Time of SHPB Dynamic Tests

Specimen Size Diameter x Length, in (cm)	Strength psi (MPa)	Modulus Mpsi (GPa)
	Concrete Compression	
4 x 8 (10.16 x 20.32)	4434 (30.58)	2.8 (26.2)
4 x 4 (10.16 x 10.16)	5868 (40.47)	4.4 (30.3)
3 x 3 (7.62 x 7.62)	4601 (31.73)	3.9 (26.9)
2 x 2 (5.08 x 5.08)	4072 (28.08)	3.6 (24.8)
	Concrete Split Tension	
4 x 4 (10.16 x 10.16)	587 (4.05)	
3 x 3 (7.62 x 7.62)	675 (4.66)	
2 x 2 (5.08 x 5.08)	586 (4.04)	
	Mortar Compression	
4 x 8 (10.16 x 20.32)	6247 (43.08)	4.5 (31.0)
3 x 3 (7.62 x 7.62)	5294 (36.51)	4.2 (29.0)
2 x 2 (5.08 x 5.08)	5959 (41.10)	4.4 (30.3)
	Mortar Split Tension	
3 x 3 (7.62 x 7.62)	746 (5.15)	
2 x 2 (5.08 x 5.08)	750 (5.17)	

Concrete Density: 2.10 g/c
Mortar Density: 2.04 g/cc

2. Crack Propagation Velocity

As discussed in Section II.2 the crack velocity of both concrete and mortar was measured using three different methods. All three methods show very complimentary results for both concrete and mortar. All the measured data are combined together in the one curve of Figure 7. Regression curves for both concrete and mortar were determined but were similar, so one regression curve is given for the combined sets of data. Approximately 150 data points are shown in Figure 7. Data obtained by John and Shah [13] and Ross et al. [14] at low strain rates are included in the data and appear to be compatible with the data obtained in this study.

It was hoped that a limiting crack velocity could be measured in this study. However, the maximum strain rate of the SHPB is on the order of 20/sec. This limitation is due to the restriction of a maximum design pressure of the 3" diameter (76.2mm) SHPB system and a limiting impact velocity of the 2" diameter (50.8mm) SHPB system.

It appears that the data and curves of Figure 7 are approaching some asymptotic value or limiting velocity. A limiting velocity of $0.38C_L$ is proposed by Broek [15] and is assumed to approach the Rayleigh wave velocity (approximately $0.6C_L$) as proposed by Anderson [16], where C_L is the longitudinal wave velocity of long bars given as

$$C_L = \sqrt{E/\rho} \qquad (6)$$

with E as Young's modulus and ρ as density. Using an average Young's modulus and density, the limiting crack velocity u_{cl} for $0.38C_L$ is 1369m/sec and for $0.6\ C_L$ the limiting crack velocity u_{cl} is 2162 m/sec.

In an effort to develop an analytical equation from the experimental data of Figure 7, a regression analysis was performed for the combined concrete and mortar. A power regression resulting in an equation for crack velocity u_c as a function of strain rate $\dot{\varepsilon}$ is expressed as

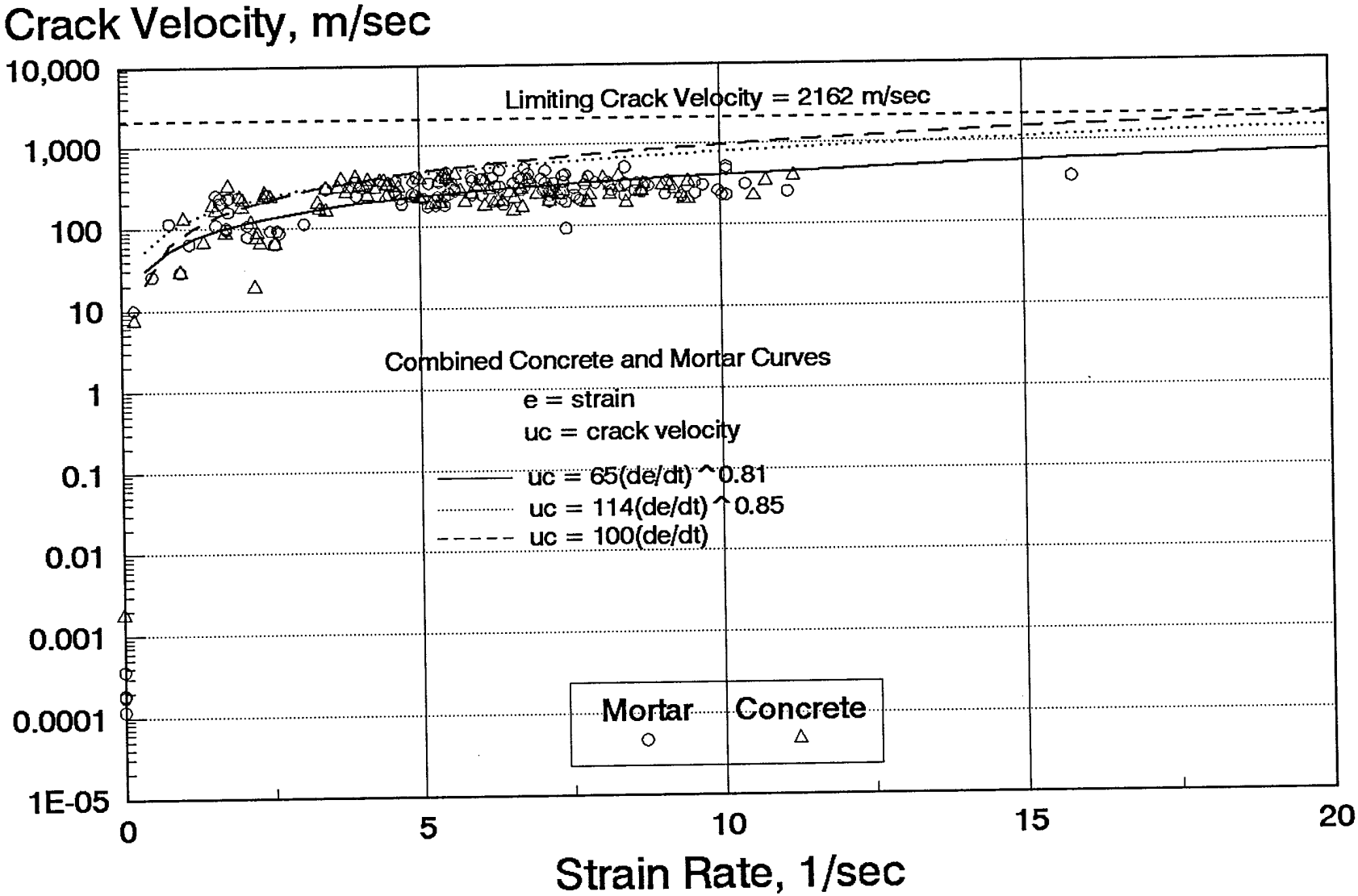

Figure 7. Crack velocity data for concrete and mortar versus strain rate.

$$u_c = k\dot{\varepsilon}^m \tag{7}$$

where log k is the log u_c intercept and m is the log u_c/log $\dot{\varepsilon}$ slope on a log u_c – log $\dot{\varepsilon}$ plot shown in Figure 8. In Figure 8, three different variations of Equation (7) are given. The solid line is the power regression curve obtained from the crack velocity as described earlier. This regression yields values of k = 65 and m = 0.81 and it is shown in Figures 7 and 8. Also shown is a regression curve of k = 114 and m = 0.85 obtained by assuming all the crack velocity obtained by the time to failure method should be approximately doubled to give an upper limit of crack velocity. The third curve of Figures 7 and 8 is based on limited crack velocity data available at the time of a publication by Ross et al. [15] and described by the parameters of k = 100 m = 1.0. Using these parameters in Equation (7) gives a rather simple linear relation of

$$u_c = 100\dot{\varepsilon} \tag{8}$$

for crack velocity as a function of strain rate. These relations will be discussed again relative to the prediction of concrete tensile strength in the next section.

Using the k,m parameters discussed above and the assumption of the curves of Figures 7 and 8 approaching a limiting crack velocity, we may calculate a strain rate at the intersection of limiting velocity and the crack velocity-strain rate curve. For the two limiting velocities and the pairs of k, m parameters the corresponding critical strain rate $\dot{\varepsilon}_{cr}$ values are given as

$$\dot{\varepsilon}_{cr} = \left(u_{Cl} / k\right)^{1/m} \tag{9}$$

and tabulated in Table 4.

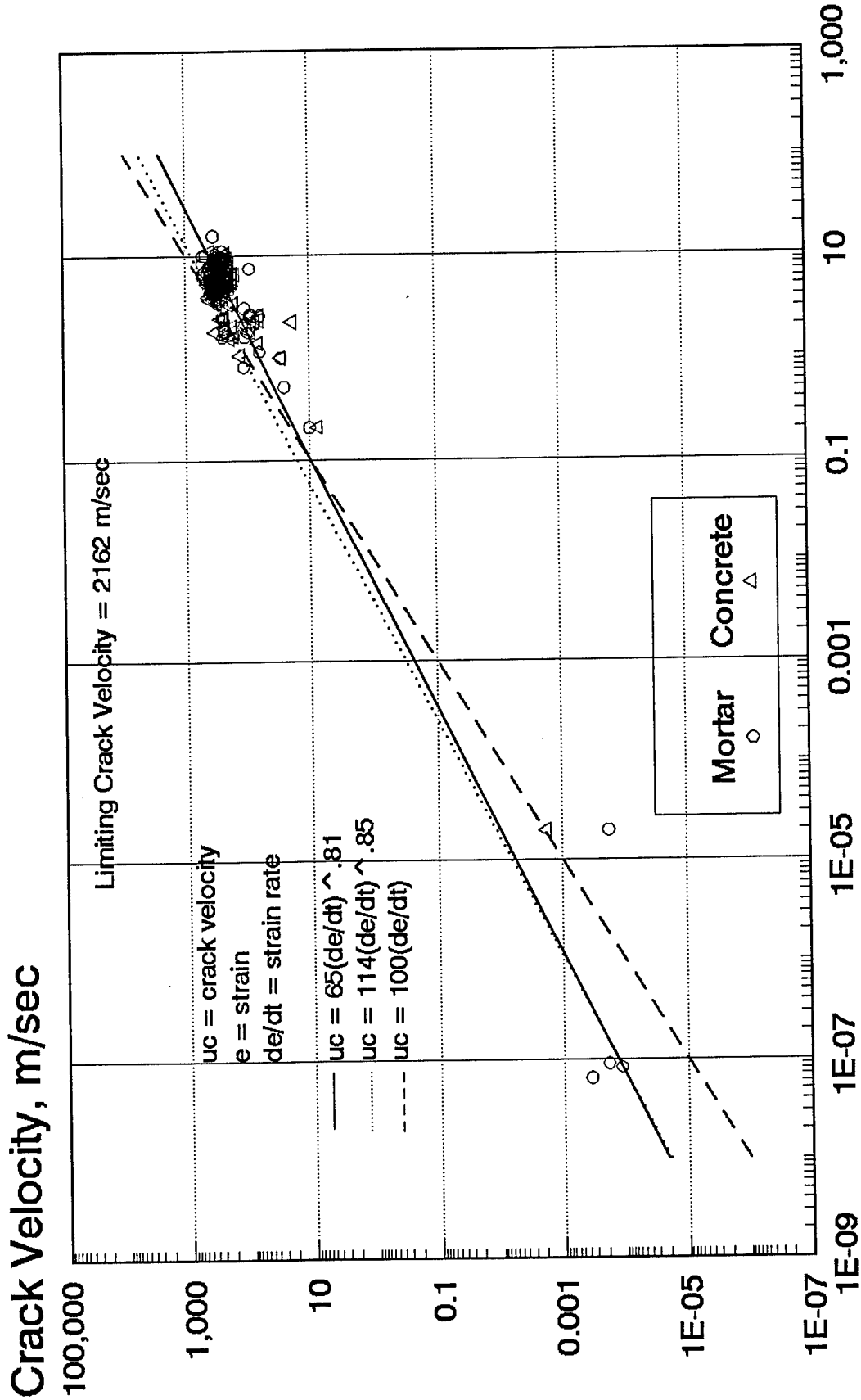

Figure 8. Log-log plot for data of Figure 7.

Table 4

Critical Strain Rate From Limiting Crack Velocity Curves

Limiting Crack Velocity = $0.38C_L$ = 1369 m/sec

Parameters	Critical Strain Rate (1/sec)
k = 65, m = 0.81	43.0
k = 114, m = 0.85	18.0
k = 100, m = 1.0	13.7

Limiting Crack Velocity = $0.6C_L$ = 2162 m/sec

Parameters	Critical Strain Rate (1/sec)
k = 65, m = 0.81	75.7
k = 114, m = 0.85	31.9
k = 100, m = 1.0	21.6

3. Tensile Strength of Concrete and Mortar

As mentioned earlier in Section II.2 the direct tension test of concrete is difficult and the splitting tension or Brazilian tests (recommend by ASTM as a standard quasistatic test) has been used in the SHPB by Ross [1, 14, 15] as an alternative dynamic tensile test specimen. Over 100 unnotched specimens were tested in the 2" diameter (50.8mm) SHPB at Tyndall AFB, FL and the 3" diameter (76.2 mm) SHPB at the University of Florida Graduate Engineering and Research Center (UFGERC) at Shalimar, FL. A series of solid unnotched cylinders of length to diameter of unity with 2", 3", and 4" diameter (50.8mm, 76.2mm and 101.6mm) were tested in the 2" diameter (50.8mm) SHPB at Tyndall AFB. Both concrete and mortar were tested using a modified loading system shown in Figure 9. The metal loading strips were fabricated to match the contour of the specimen on one side and flat to match the end of SHPB on the other side. The loading strip width was variable with a width to specimen diameter of 0.2 based on experiments by Tang et al. [11, 12]. Length of the loading strips was always the same length as that of the specimen. An additional series of 2" and 3" diameter (50.8mm and 76.2mm) specimens, with

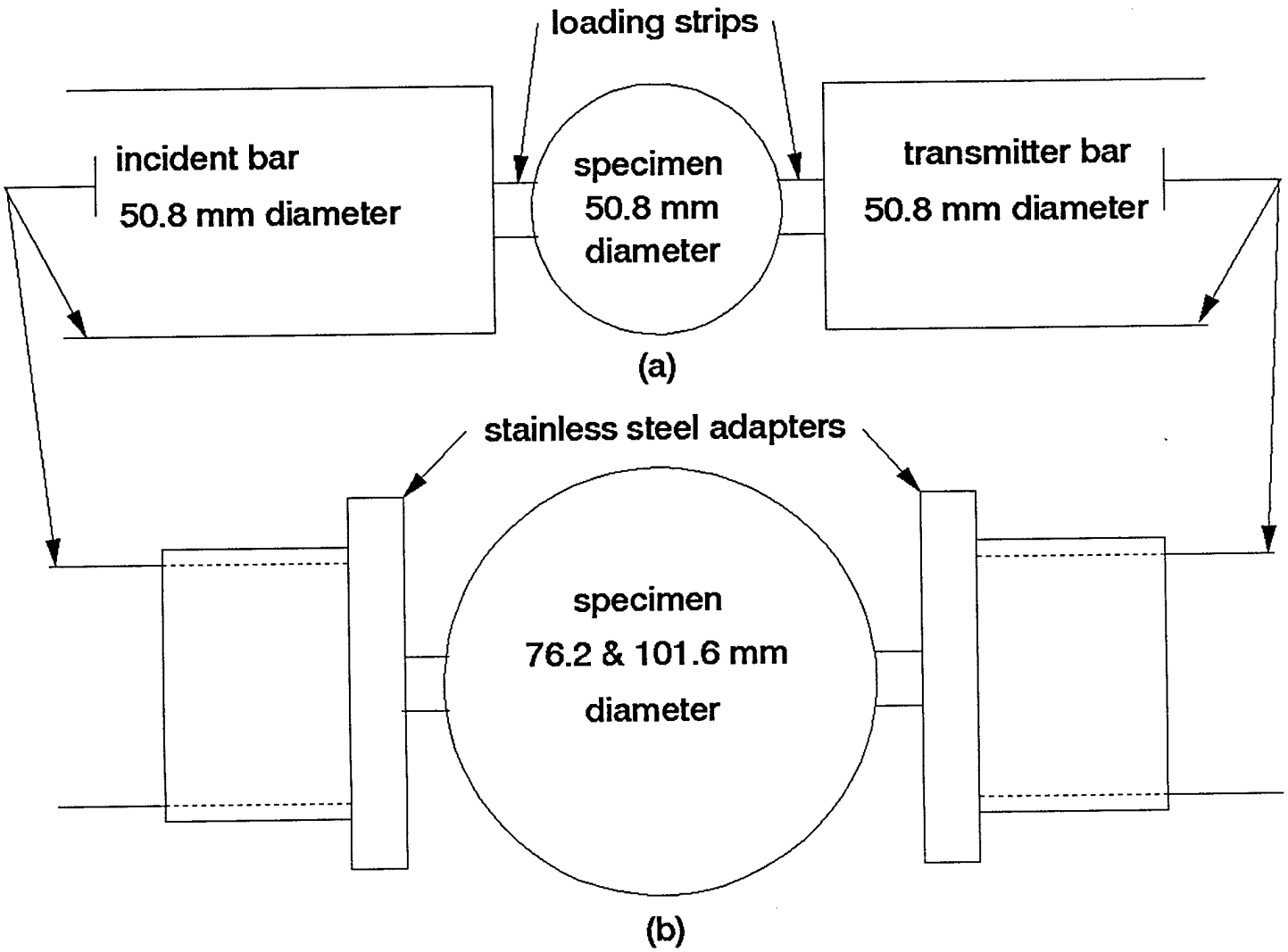

Figure 9. Schematic of modiifcation of 2" diameter (50.8 mm) SHPB for testing of 3" and 4" diameter (76.2 and 101.6 mm) specimens.

length equal to diameter, were tested in the 3" diameter SHPB at University of Florida Graduate Engineering and Research Center (UFGERC). Again, both concrete and mortar were tested using metal loading strips. These two series of tests gives a combination of two cementitious materials, three specimen sizes and two SHPB systems. These data are shown as a dynamic to static strength ratio plotted versus log (strain-rate, 1/sec) in Figure 10. In addition, data of five different mixes of concrete of a fixed size [17] and data from an experiment by Birkimir [16] are also included. Data for the different mixes was obtained using the 2" diameter SHPB, whereas the data of Birkimir was obtained using metal projectile impact on long concrete rods instrumented with electrical resistance strain gages as shown in Figure 11. These two sets of data are included to fill out an interesting collection of data that have similar characteristics. This means there are at least eight different cementitious materials, four different size specimens, two different diameter SHPB's and one additional test method producing tensile data, all showing the same trend.

One of the major objectives of this research was to determine crack velocity of cementitious material and apply that data to the prediction of tensile strength. The following is an attempt to tie two independent experiments together to produce an analytical expression for the dynamic increase factor (DIF) defined as the ratio of the tensile strength at strain rate divided by the quasistatic tensile strength. A low strain rate of approximately 10^{-6}/sec was used as the quasistatic strain rate.

Grady [19] and Grady and Kipp [20] recognized that at the higher strain rates above 1/sec, rock and cementitious material such as concrete showed a slope on a log σ_t – log $\dot{\varepsilon}$ plot of approximately 1/3. Studies by Grady [19] on brittle fracture of condensed matter are based on the assumption that local kinetic energy plus strain energy must exceed or equal the fracture surface

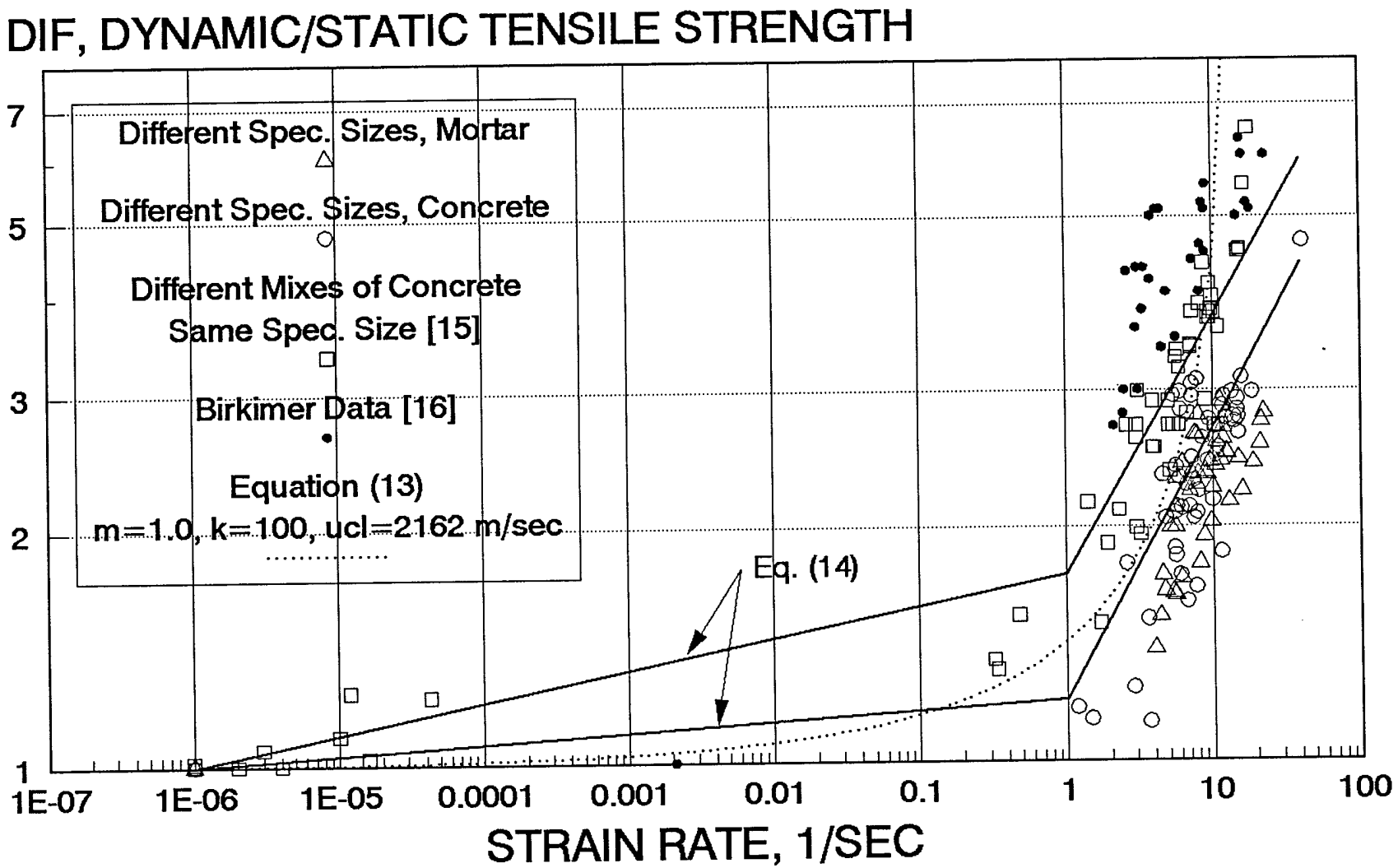

Figure 10. Strain rate effects of concrete and mortar using splitting tensile tests to determine tensile strength.

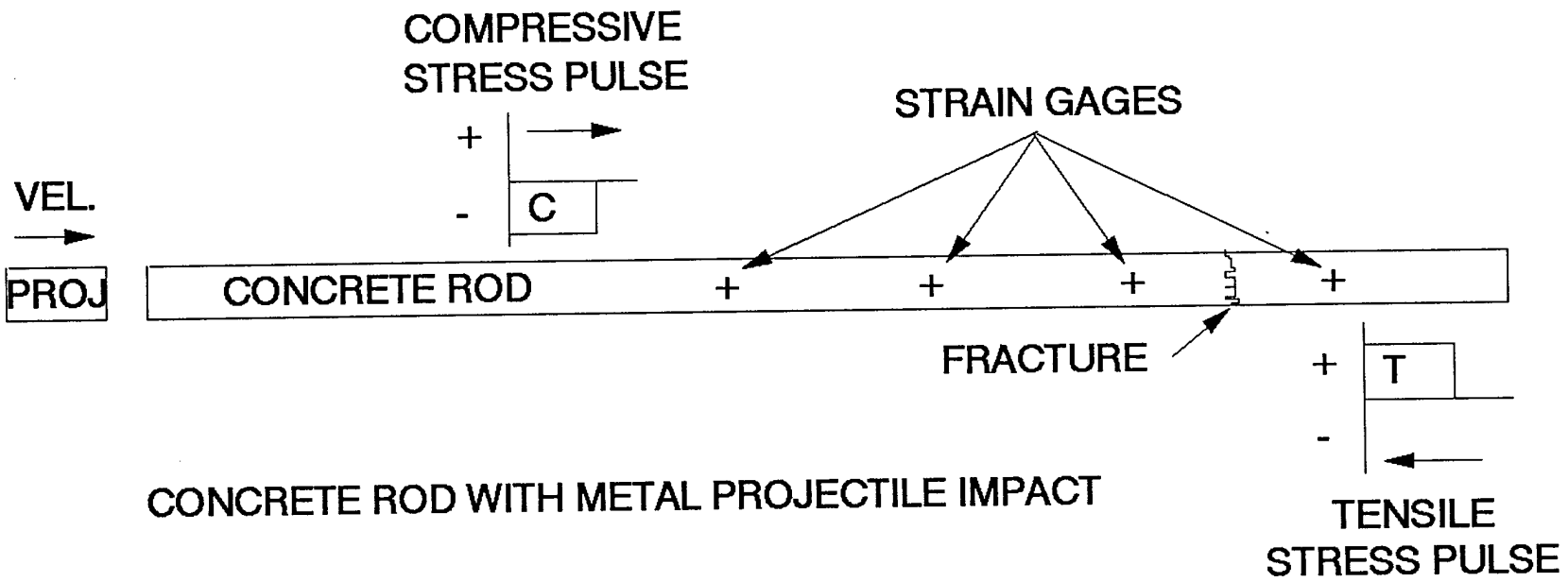

Figure 11. Test arrangement used by Birkimer [16].

energy for fracture to occur. Grady's basic equation for tensile strength σ_s of brittle material is given as

$$\sigma_s = \left(3\rho c_o K_{IC}^2 \dot{\varepsilon}\right)^{1/3} \tag{10}$$

where ρ = material density

c_o = wave velocity

K_{IC} = static fracture toughness

$\dot{\varepsilon}$ = strain rate > 1.0/sec.

Grady's equation (10) assumes the static fracture toughness K_{IC} is constant and that cracks grow at a rate equal to the wave speed c_o. Ross et al. [17] modified this equation to account for crack velocity as a function of strain rate, given by Equation (7) and account for changes in fracture toughness as suggested by Anderson [16]. Dynamic fracture toughness K_{ID} as suggested by Anderson is given by

$$K_{ID} = K_{IA} / \left[1 - \left(u_c / u_{cl}\right)^n\right] \tag{11}$$

where K_{IA}= arrest fracture toughness

u_c = crack velocity

u_{cl} = limiting crack velocity

n = 1/3 to ½ [17].

Equation (11) presents a problem as it produces an infinite K_{ID} at $u_c = u_{cl}$. This problem is discussed later relative to a critical strain rate.

Using Equations (7, 10, 11) and the assumption of crack velocity controlling crack growth a modified Grady equation for tensile strength σ_t of brittle materials is written as

$$\sigma_t = \left\{ \left(3K_{IA}^2 B\right)\dot{\varepsilon}^{1-m} / k\left[1-\left(\frac{k\dot{\varepsilon}^m}{u_{cl}}\right)^n\right]^2 \right\}^{1/3} \qquad (12)$$

where B = bulk modulus and other parameters have been defined previously. It is suggested by Anderson [16] that the arrest fracture toughness is approximately 25 percent of the static fracture toughness K_{IC}.

If the DIF (strength at strain rate divided by quasistatic strength) is formed by dividing Equation (1) by itself when $\dot{\varepsilon} = \dot{\varepsilon}_o$, quasistatic strain rate, gives an analytical expression equivalent to the normalized stress ratio found using the experimental data. This ratio eliminates the need for knowing K_{IA} and produces an expression which when used with the quasistatic tensile strength predicts the tensile strength of concrete or a brittle material at a strain rate of interest. This expression may be written as

$$\frac{\sigma_t}{\sigma_o} = \mathrm{DIF} = \left(\frac{\dot{\varepsilon}}{\dot{\varepsilon}_o}\right)^{\frac{1-m}{3}} \left\{ \left[1-\left(\frac{k\dot{\varepsilon}_o^m}{u_{cl}}\right)\right]^{\frac{1}{3}} \Big/ \left[1-\left(\frac{k\dot{\varepsilon}^m}{u_{cl}}\right)^{\frac{1}{3}}\right] \right\}^{\frac{2}{3}} \qquad (13)$$

where σ_o is the quasistatic tensile strength, $\dot{\varepsilon}_o$ is the strain rate used in obtaining σ_o, and the other parameters are defined previously. The better fit for this type equation with respect to the normalized experimental data of Figure 10, is for the following parameters of $\dot{\varepsilon}_o = 1 \times 10^{-6}$/sec, k = 100, m = 1.0, and u_{cl} = 2162 m/sec. This equation is shown as the dotted curve of Figure 10. DIF curves generated using regression parameters from the other two curves of Figures 7 and 8 do not match the experimental data as well as that of the DIF curve of Figure 10. If the general approach of using expressions such as Equations (11, 12, 13) is correct then one solution would be better verification of the crack velocity at the low and high strain rates as well as measurement of crack velocities at the intermediate strain rates between 10^{-5} to 10^{-2}/sec.

Additional methods of predicting concrete tensile strength are empirical methods used by a European-International Committee on Concrete (Comite' Euro-International du Beton, CEB [21]). This prediction is based on experimental data obtained by researchers such as Kormeling et al. [6], Reinhardt [22, 23, 24] and Weerheijm [25, 26]. Modified equations for the empirical prediction are presented by Malvar and Ross [27] and are given as

$$\frac{\sigma_t}{\sigma_o} = \mathrm{DIF} = \left(\frac{\dot{\varepsilon}}{\varepsilon_o}\right)^{\delta} \quad \text{for } \dot{\varepsilon} \le 1/\sec$$
$$= \beta\left(\frac{\varepsilon}{\varepsilon_o}\right)^{1/3} \quad \text{for } \dot{\varepsilon} > 1/\sec \qquad (14)$$

where σ_t = dynamic tensile strength at $\dot{\varepsilon}$

σ_o= quasistatic tensile strength at $\dot{\varepsilon}_o$

$\dot{\varepsilon}_o = 10^{-6}$/sec (quasistatic strain rate)

$\log \beta = 6\delta - 2$

$\delta = 1/\left[1 + 8\left(f_c^1 / f_{co}^1\right)\right]$

$f_{co}^1 = 10$ MPa = 1450 psi

f_c^1 = compressive strength of concrete being considered.

Equation (14) for concrete f_c^1 = 30 MPa and 70 MPa (4350 – 10,150 psi) are shown as solid bilinear lines in the Figure 10 log-log plot. These lines show reasonable correlation with the experimental data of Figure 10.

Considerable more experimental data is available in the low, intermediate and high strain rates. Cowell [27] presents both low and intermediate strain rate data for three different concrete compressive strengths between 32 and 63 MPa. Kvirikadze [29] presents both low and intermediate strain rate data for a compressive strength concrete of 23 MPa. Takeda and

Tachikawa [30] presents low and intermediate strain rate data for a concrete with an unknown compressive strength. The Birkimer [18] data was obtained using concrete compressive strength of 47 MPa. The Kormerling et al. [6] tensile strength data was obtained using a 3" diameter (76.2mm) gravity driven SHPB up to strain rates of 1.5/sec. Ross [1] reports direct tension data obtained using a 2" diameter (50.8mm) SHPB which shows the same trends of Figure 10. John et al. [31] presents high strain data from a large SHPB using concrete with a compressive strength of 53 MPa. Antoun [32] used concrete with a compressive strength of 57MPa and a large SHPB to produce high strain rate data. The highest DIF reported in the literature by McVay [33] is approximately 7.0 at a strain rate on the order of 50/sec. The McVay data was back calculated using spall velocity data from the back side of a concrete wall subjected to a front face blast loading.

All the concrete tensile strength found in the literature falls within a DIF-strain rate region approximated by the cross hatched area of Figure 12. Shown also are the modified CEB lines as well as the analytical curve shown in Figure 10. The CEB lines reflect the result of tests by Reinhardt [22, 23, 24] which tend to show generally that concrete of lower strength or maturity exhibit a higher strain rate sensitivity than that of the high strength concrete. This is realized by the two CEB lines which show the lower compressive strength concrete to have a higher DIF for a given strain rate than that of the higher strength concrete. This observation was also reported by Cowell [28] in his tests of concrete in the lower and intermediate strain rate range. This trend is reflected in the mortar and concrete data of Figure 10 where the mortar has a higher compressive strength than that of the concrete. The data of Birkimer [18] of Figure 10 does not conform to this trend, but one must remember the Birkimer data was obtained using a different test method than that of all the other data shown.

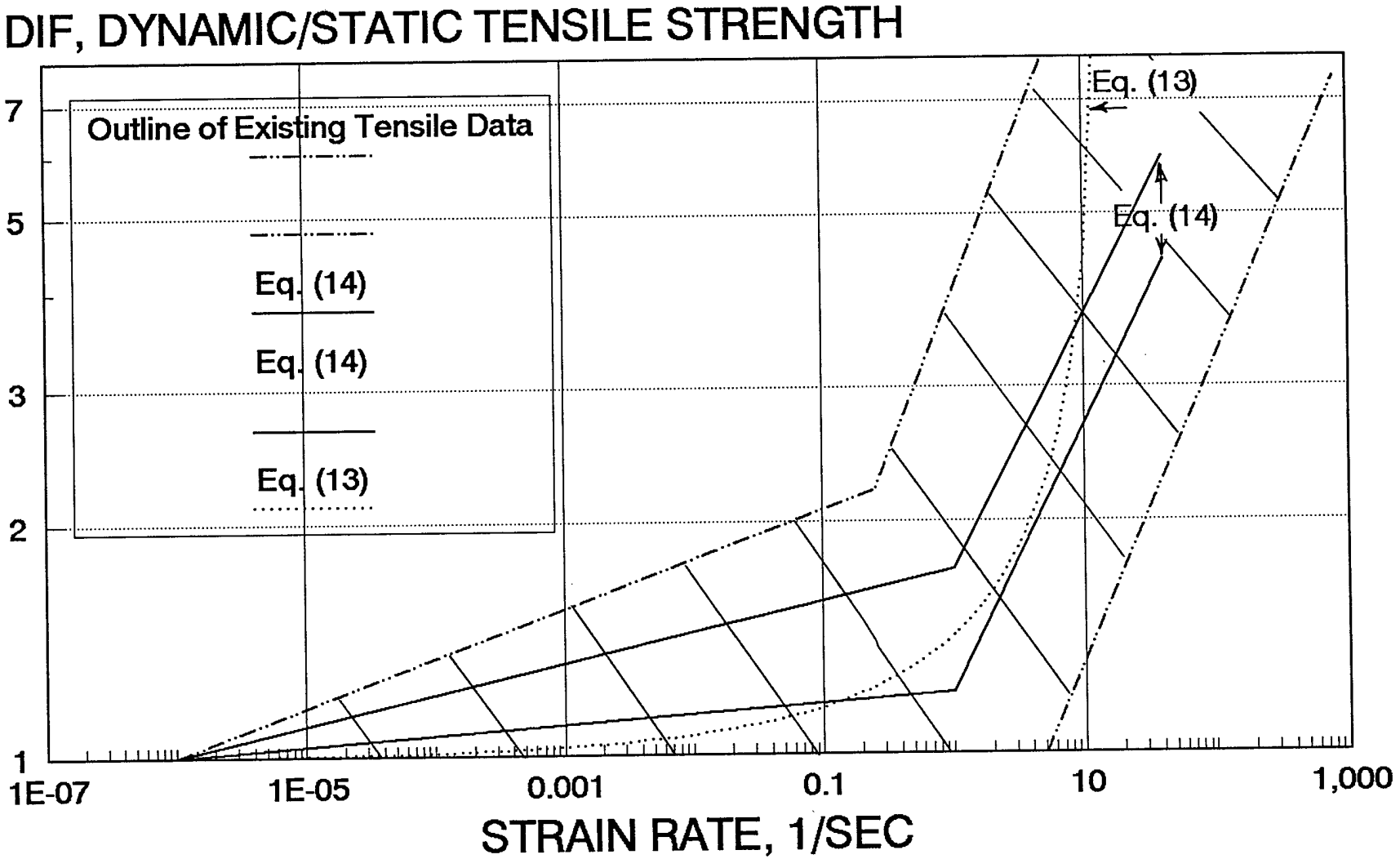

Figure 12. Sketch showing extent of concrete tensile data.

4. Effects Of Dynamic Precompression On Tensile Strength

A series of 50.8mm mortar specimens were loaded, with increasing load rate, in the 2" diameter (50.8mm) SHPB at the Air Force Research Laboratory, Tyndall AFB, FL. (See schematic of Figures 1 and 13a.) Three iterations of each load rate were tested for five different load rates. Compression failure was assumed when multiple visible cracking was observed on the cylinder and in some cases pieces were expelled from the surface of the specimen. The failure stress for the 50.8mm diameter specimens was taken at 46.2 MPa and 55.5 MPa for the 76.2 diameter specimens. For this kind of loading a tendency toward longitudinal cracking has been determined experimentally by Malvern et al. [34] and Ross [35]. In reality the cracking pattern is bowed slightly away for the longitudinal axis and initially occurs close to the outside surface and the amount of cracking increases as the strain rate increases. Wave velocity measurements, in the specimen longitudinal direction, were made on the 50.8mm diameter specimens both before and after the precompression loading. The 50.8mm diameter specimens were also tested in a splitting tensile mode using the 50.8mm diameter SHPB by rotating the cylindrical specimen 180° as shown schematically in Figure 1c and 13b. This type dynamic loading is analyzed and described in detail by Tedesco et al. [36] and the mode of failure is longitudinal splitting along a diametrical plane containing the load as shown in Figure 13b. For the splitting tensile tests, after precompression and wave velocity measurements, the loading rate was kept constant to obtain a variable tensile strength for a variable precompression stress.

In an attempt to determine whether wave velocity after precompression was different in the transverse direction than that of the wave velocity in the longitudinal direction, a series of 76.2mm diameter specimens were tested in the 76.2mm diameter SHPB at the University of Florida Graduate Engineering and Research Center (UFGERC) Shalimar, FL. Wave velocity

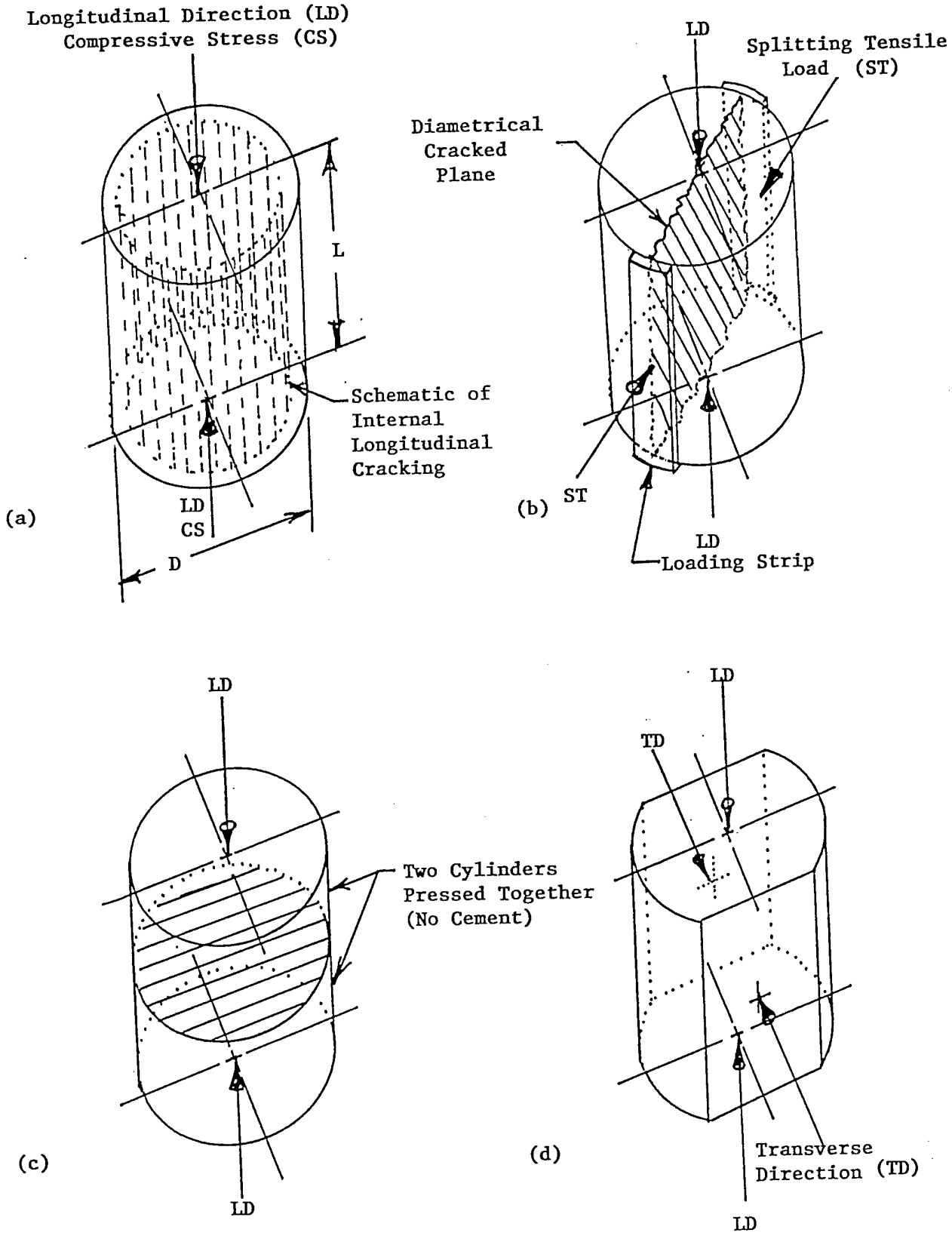

Figure 13. Schematic of experimental test cylinders, (a) dynamic compression, (b) splitting tensile mode, (c) simulated crack plane, and (d) sawed plane for transverse direction wave velocity measurement. D = specimen diameter, L = specimen length

measurements in the longitudinal direction were taken for all 76.2mm diameter specimens prior to precompression. One specimen was ground flat on opposite sides in order to measure the transverse direction velocity with no precompression. After precompression of the 76.2mm diameter specimens a flat was sawed on these specimens to facilitate wave velocity measurements in the transverse direction as shown in Figure 1d. Wave velocity measurements were made in both the longitudinal and transverse directions of the 76.2mm diameter specimens after the precompression loading. All velocity measurements were made using a 150kHz transducer set. For the 50.8mm diameter specimens the transit time was approximately twice the natural period of the transducer and for the 76.2mm specimens the transit times was approximately three times the natural period of the transducer.

One measure of damage for the mortar specimens was thought to be the ratio of tensile strength for a given precompression stress to the tensile strength for a similar specimen prior to a precompression stress. The tensile strength for specimens without precompression was determined by testing several cylinders with no precompression in the split tension mode in the 50.8mm diameter SHPB. The residual strength of the specimens was also determined in the same manner. A tensile strength ratio, i.e. tensile strength with precompression stress divided by tensile strength with no precompression stress was determined for each of the 50.8mm diameter specimens. These values are shown plotted versus a compression stress ratio in Figure 14. Since the failure compression stress was different for the two different size specimens and SHPB's, probably due to size effects, a compression stress ratio was defined as the ratio of the precompression stress for the specimen divided by the failure compression stress. In comparison the tensile strength ratio will be unity for a compressive stress ratio of zero and the tensile strength ratio is expected to decrease as the compressive stress ratio increases. The data of Figure 14

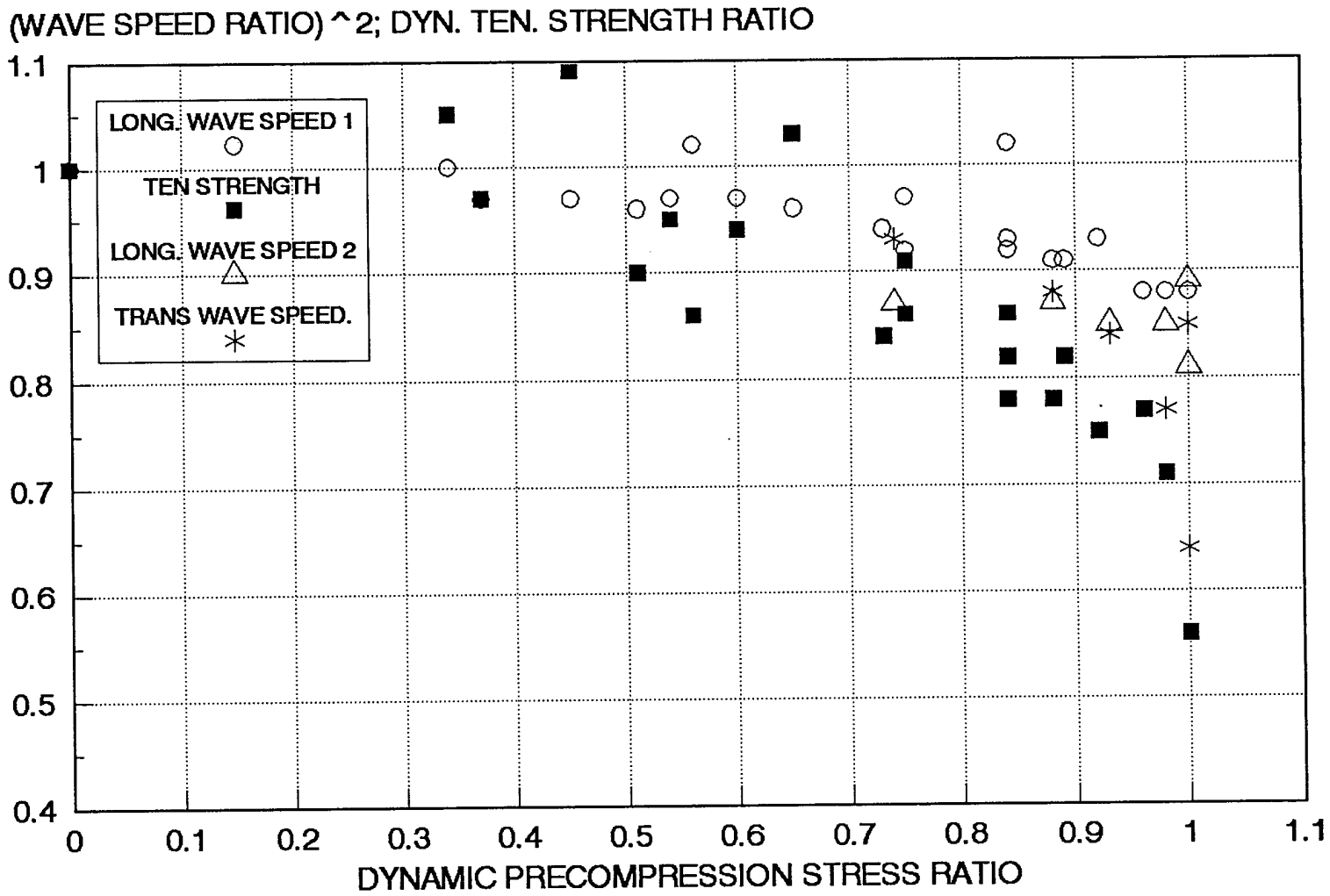

Figure 14. Effect of dynamic precompression stress on transverse dynamic tensile strength ratio and the wave velocity ratio squared.

shows a rather gradual decrease in tensile strength up to an approximate compression ratio of 0.8, but as the compression ratio approaches 1.0 the tensile strength decreases drastically theoretically approaching zero when the specimen is fractured into several pieces.

When we consider some damage ratio in terms of wave velocity measurements, the modulus or stiffness ratio based on the square of wave velocity, may be the better measure of damage. The square of elastic-stress wave velocity c for a longitudinal wave in an unbounded isotropic medium is given as

$$c^2 = \frac{\lambda + 2\mu}{\rho} = \frac{E(1-\upsilon)}{\rho(1+\upsilon)(1-2\upsilon)} \tag{15}$$

Where c = wave velocity (unbounded medium)

λ, μ = Lame's constants

$\mu = G$ = Shear modulus

E = Young's modulus

υ = Poisson's ratio

ρ = material density

For the unbounded medium dispersion effects are zero and for long rods where the wave length is large compared to the diameter the dispersion effects may be neglected. The stress wave velocity c_o for isotropic elastic long rods is

$$c_o^2 = \frac{E}{\rho}. \tag{16}$$

All wave velocity measurements were made using a transducer that produced longitudinal waves with particle motion in the direction of the wave motion. When the words longitudinal direction and transverse direction are used they are simply describing a direction of measurement; all waves used in these tests are longitudinal waves.

If we use a modulus or stiffness ratio as a description for damage, then the square of the ratio of the wave velocity of a damaged specimen to that of an undamaged specimen may be used as a modulus or stiffness ratio. Since the specimens are bounded and are not long rods, it is not clear as to what stiffness ratio is represented by the square of the wave velocities. However, the ratio of the velocities squared is thought to be a better representation of a damage parameter than the ratio of the wave velocities. Shown in Figure 14 and marked as "long wave speed 1" the square of the ratio of wave velocities, taken in the longitudinal direction of the smaller specimens (see Figure 13), shows a decrease in value as the compression ratio increases. However, this decrease is not near as severe as the tensile strength ratio decrease in the same specimens. The difference in these two values was attributed to the fact that the damage from the precompression stress is cracking running almost parallel to the longitudinal specimen direction and is almost invisible to the longitudinal wave motion of the test transducer. To reinforce this conclusion a wave velocity measurement was made on specimens as shown in Figure 13b and 13c. For the specimen of Figure 13b the transducers were placed so as to straddle the diametrical cracked plane and in Figure 13c, a single cracked plane, simulated by placing two specimens in series was formed normal to the wave motion. Wave velocity measurements for those experiments differed only slightly from measurement on damage free specimens. But, in the case of the tensile failure the multiple cracking caused by the precompression pulse is parallel to the tensile failure plane and has the effect of reducing the tensile strength.

In order to try and prove experimentally that multiple-cracked planes would degrade wave velocity measurements made transverse to the cracked planes, as opposed to measurements made parallel to the plane, a series of 76.2mm specimens were exposed to a dynamic precompression pulse and then sawed as shown in Figure 13d. Wave velocity measurements were made in the

longitudinal direction of all specimens prior to dynamic precompression. A sample undamaged specimen with ground parallel sides was measured for wave velocity in both the transverse and longitudinal directions as shown in Figure 13d. Appreciable differences were found between these transverse direction measurements and the longitudinal direction wave measurements of both sizes of damaged specimens.

The data for the square of the wave velocity ratio for the longitudinal direction and for the transverse direction of the larger specimens are shown versus the compression stress ratio of Figure 14. The square of the wave velocity ratio for the longitudinal direction of the larger specimens is marked as "long wave speed 2"and the square of the velocity ratio for the transverse direction of the same specimens is marked as "trans wave speed." For these data the square of the wave velocity ratio for measurement in the transverse direction show almost the same trend as the dynamic tensile strength ratio given for the 50.8mm diameter tested previously. The square of the wave velocity ratio for measurements made in the longitudinal directions show very similar trends as the corresponding data for the 50.8mm diameter specimens. The measured wave velocity in the undamaged specimens averages 3.6 km/sec.

The basic question of whether a compression pulse traversing a concrete or mortar specimen causes significant tensile strength reduction has been answered for a concrete cylinder. For concrete cylinders loaded axially in a SHPB, longitudinal cracking occurs and reduces the tensile strength when measured in the transverse direction. However, this does not specifically answer the question of what effect does a purely compressional pulse have on an unbounded medium without free surfaces. The results do reemphasize that concrete damage is directional and not simply a scaler function.

5. Dynamic Fracture Toughness

Forty notched concrete and mortar specimens (shown schematically in Figures 2 and 4) were tested quasistatically and fracture toughness of each material was determined using the peak load method by Tang et al. [37]. Fracture toughness values of mortar and concrete at a strain rate of 1 x 10^{-7}/sec are given in Table 5. These values agree reasonably well with values presented by Tang et al. [37] and Shah [38].

Table 5
Quasistatic Fracture Toughness for Concrete
and Mortar at a Strain Rate of 1 x 10^{-7}/sec

Specimen Size	K_{IC}^{s} MPa – $m^{1/2}$	
Diameter x Length, in (mm)	Concrete	Mortar
3 x 1 (76.2 x 25.4)	0.58	0.74
2 x 2 (50.8 x 50.8)	0.68	0.77
3 x 3 (76.2 x 76.2)	0.70	0.93

Over 150 notched concrete and mortar specimens were tested at variable strain rates in the 3" diameter (76.2mm) UFGERC SHPB. High-speed photography, as shown in Figure 15, was used to observe the crack motion during specimen failure. The peak load method of Tang et al. [36] was used to evaluate the dynamic fracture toughness for dynamic loading. The dynamic fracture toughness analysis was inconclusive. Based on this, three different sizes of hole notched cylindrical specimens were fabricated for dynamic SHPB tests. These specimens were to be tested as splitting tensile specimen in the UFGERC SHPB. However, the high speed camera malfunctioned just prior to completion of these tests and the fracture toughness test and final analysis were not completed in time for inclusion in this report.

6. Moisture Effects on Tensile Strength of Concrete

Moisture effects coupled with strain rate effects have been reported by Ross et al. [17]. Tests were conducted on water saturated and partially saturated splitting tensile specimens in the

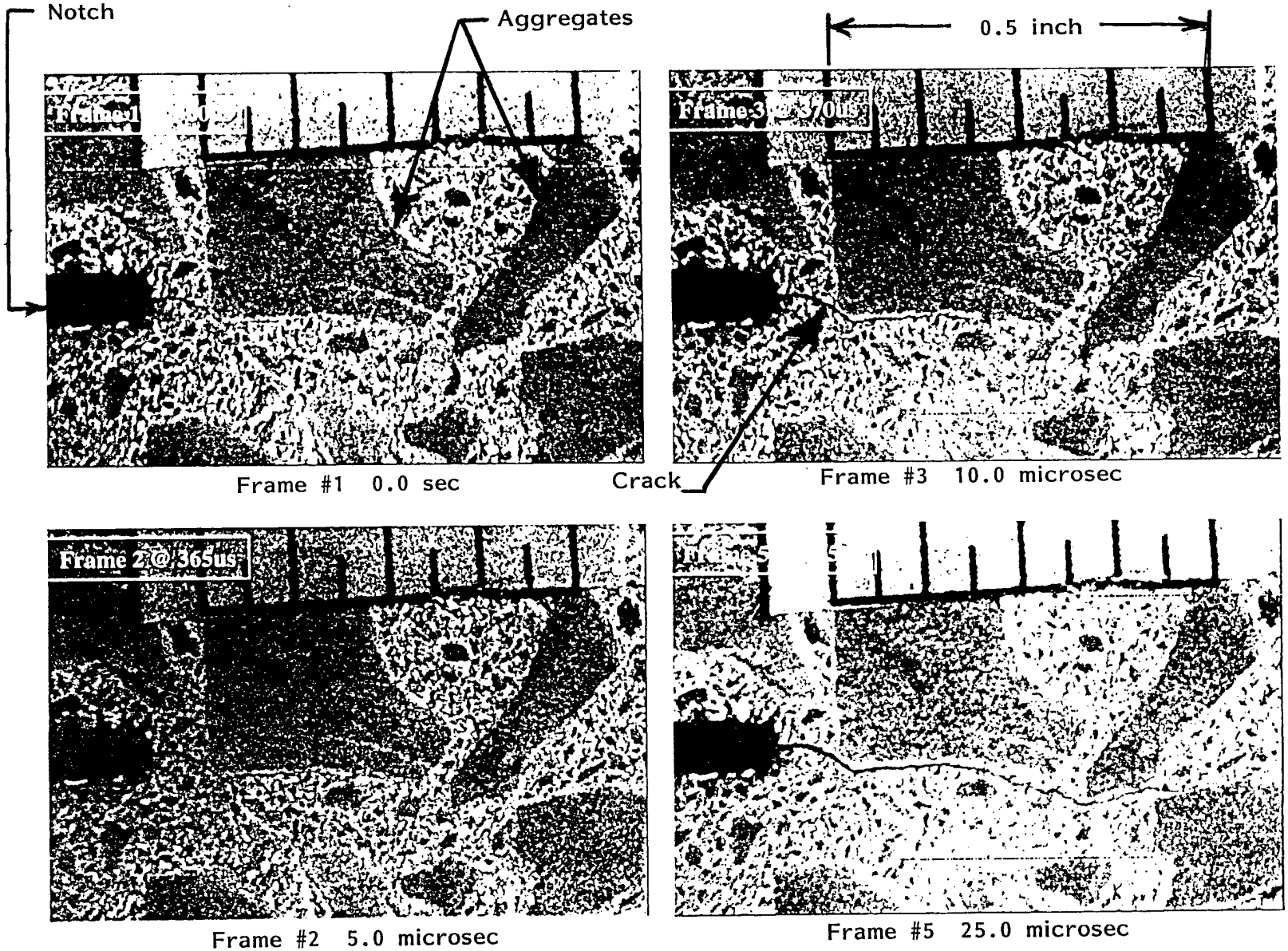

Figure 15. High-speed photography of crack propagation in a concrete specimen 5.0 microsec between frames with 80 nanosec exposure time.

2" diameter (50.8mm) SHPB. Quasistatic properties of the wet specimens showed reduced values when compared to dry specimens of the same material. This reduced strength at quasistatic strain rates is well known and reported by Neville [9]. The effects of moisture at the higher strain rates may then be attributed to the reduced strength at quasistatic strain rates, similar to differences in dynamic response of concrete having different strengths, reported by Reinhardt [22, 23, 24].

In an effort to investigate the combined effects of moisture and strain rate, for this study, a series of different size hole notched cylindrical specimens (to be used in conjunction with fracture toughness of dry specimens) were fabricated and placed in water after casting. These wet specimens were to be tested along with dry specimens to determine tensile strength, crack velocity, and fracture toughness. As mentioned above the high-speed camera malfunction prevented the testing of these specimens in time for inclusion in this report.

IV. CONCLUSIONS AND RECOMMENDATIONS

Experimental tests by many researchers, and verified in this study, show that the effects of increased strain or load rates on concrete give rise to significant increases in the tensile strength. Tensile strength increases of concrete and mortar show a gradual rise in strength at strain rates below 10^{-6}/sec up to strain rates of approximately 1.0/sec. Tensile strength increases as high as 1.5 to 2.0 times the quasistatic tensile strength are reported in this region. At strain rates above 1.0/sec a significant and rather abrupt increase in tensile strength is observed. Tensile strength increases in the range of 1.0/sec to 50/sec are reported to increase 2.0 to 7.0 times the quasistatic value. Measured crack velocities when coupled with analytical procedures correlate very well with the experimental evidence.

Measured crack velocities for various high strain rates, of this study, tend to show a tendency to become asymptotic to a limiting crack velocity. Measured concrete and mortar crack velocities at strain rates of 1 to 10/sec are on the order of twenty-five to fifty percent of the calculated limiting crack velocity based on a limiting crack velocity of 0.6 $\sqrt{E/\rho}$ (bar wave velocity). If compared to the 0.38 $\sqrt{E/\rho}$, then the measured crack velocities are on the order of 40 to 80 percent of the calculated limiting crack velocity.

Testing, using dynamic precompression pulses prior to tensile testing in the SHPB produce longitudinal cracking, which reduces concrete tensile strength with increases in the precompression stress. Ultrasonic stress wave velocity measurement transverse to the cracking tend to verify the damage due to cracking. Squared ratios of wave velocity before and after precompression are better indicators of stiffness or modulus damage than that of the ratio of wave velocities. The critical wave velocity reduction indicating severe damage is approximately thirty percent of the undamaged wave velocity.

Dynamic fracture of material parameters show increases with strain rate or loading rate and study in this area should be continued. Dynamic fracture toughness parameters as function of strain rate should lead to a better understanding of the effects of strain rate on concrete tensile strength.

V. REFERENCES

1. Ross, C. A., "Split Hopkinson Pressure Bar Tests," ESL-TR-88-82, HQAF Engineering and Services Center, Tyndall AFB, FL, March 1989.

2. Malvern, L. E. and Ross, C. A., "Dynamic Response of Concrete and Concrete Structures," two annual reports and a final report for AFOSR Grant F49620-83-K007, University of Florida, Gainesville, FL, Feb. 1984, Feb. 1985, and May 1986.

3. Kolsky, H., "Investigation of the Mechanical Properties of Materials at High Strain Rates of Loading," Proc. of the Phy. Sco., Sect. B, Vol. 62, 1949, pp. 676 – 704.

4. Hopkinson, B., "A Method of Measuring the Pressure Produced in the Detonation of High Explosives or by the Impact of Bullets," Phil. Trans. Royal Soc. of London, A, 1914, pp. 437 – 456.

5. Nicholas, T., Material Behavior at High Strain Rates, Impact Dynamics, J. Wiley & Sons, NY, 1982, pp. 277 – 332.

6. Kormeling, H. A., Zielinski, A. J., and Reinhardt, H. W., "Experiments on Concrete under Single and Repeated Uniaxial Impact Tensile Loading," Stevin Lab. Report 5-80-3, Delft University of Technology, 2nd Printing, 1981.

7. Tedesco, J. W., Ross, C. A., and Brunair, R. M., "Numerical Analusis of Dynamic Split Cylinder Tests," Computers & Structures, V. 32, No. 3-4, 1989, pp. 609 – 624.

8. Timoshenko, S. P. and Goodier, J. N., Theory of Elesticity", 3rd Edition, Mc-Graw-Hill, NY, 1970, p. 123.

9. Neville, A. M., Properties of Concrete, 3rd Edition, J. Wiley & Sons, NY, 1993, pp. 529 – 565.

10. American Concrete Institute, ACI Bldg. Code, 1977.

11. Tang, T., "Effects of Load-Distributed Width on Split Tension of Unnotched and Notched Cylindrical Specimens," J. Test & Evaluation, 22-5, 1994, pp. 401- 409.

12. Tang, T., Bazant, Z., Yang, S. and Zollinger, D., "Variable-Notch One-Size Test Method for Fracture Energy and Process Zone Length," Eng. Fract. Mech., 55-3, pp. 383 – 404, 1996.

13. John, R. and Shah, S. P., "Fracture of Concrete Subjected to Impact Loading," Cement, Concrete and Aggregates, CCAGDP, Vol. 8, No. 1, Jan. – Feb.1986, pp. 24 – 32.

14. Ross, C. A., Tedesco, J. W., and Kuennen, S. "Effects of Strain Rate on Concrete Strength", ACI Materials Journal, Vol. 92, No. 1, Jan. – Feb.1995, pp. 37-47.

15. Broek, D., Elementary Engineering Fracture Mechanics, M. Nijhoff Publ., Boston, 1982.

16. Anderson, T. L., Fracture Mechanics: Fundamentals and Applications, CRC Press, Boca Raton, FL, 1991.

17. Ross, C. A., Jerome, D. M., Tedesco, J. W., and Hughes, M. L., "Moisture and Strain Rate Effects on Concrete Strength," ACI Materials J., Vol. 93, No. 3, May – June 1996, pp. 293 – 300, 1996.

18. Birkimer, D. L., "Critical Normal Fracture Strain of Portland Cement Concrete," Ph.D. Dissertation, University of Cincinnati, 1968.

19. Grady, D. E., "The Spall Strength of Condensed Matter," J. Mech. & Phys. of Solids 36-3, 1988, pp. 353 – 384.

20. Grady, D. E. and Lipkin, J., "Criteria for Impulsive Rock Fracture," Geophy. Res. Letters, V. 7, No. 4, April 1980, pp. 255 – 258.

21. Comite' Euro-International du Beton, CEB-FIP Model Code 19990, Redwood Books, Trowbridge, Wilthsire, UK, 1993.

22. Reinhardt, H. W., "Strain Rate Effects on the Tensile Strength of Concrete as Predicted by Thermodynamics and Fracture Mechanics Models," Cement Based Composites: Strain Rate Effects on Fracture, Mindess and Shah, editors, Dec. 1995, pp. 1 – 13.

23. Reinhardt, H.W., "Tensile Fracture of Concrete at High Rates of Loading", Applications of Fracture Mechanics to Cementitious Composites, Shah, S.P., Editor, Martinus Nijoff, The Hague, Netherlands, 1985, pp. 559-590.

24. Reinhardt, H.W., "Concrete Under Impact Loading-Tensile Strength and Bond," HERON, Vol. 27, No. 3, 1982.

25. Weerheijm, J. and Reinhardt, H.W., "Modeling of Concrete Fracture Under Dynamic Loading," Fracture of Rock and Concrete – Recent Developments, Shah, Swartz, and Barr, editors, 1989, pp. 721 – 728.

26. Weerheijm, J., Concrete Under Impact Tensile Loading and Lateral Compression, PhD Dissertation, Delft University of Technology, Delft, Netherlands, 1992.

27. Malvar, L. J., and Ross, C. A., "Review of Strain Rate Effects for Concrete in Tension," accepted for publication in the ACI Materials Journal.

28. Cowell, W. L., "Dynamic Properties of Plain Portland Cement Concrete," Tech. Report R447, NCEL, Port Hueneme, CA, 1966.

29. Kvirikadze, O. P., "Determination of the Ultimate Strength and Modulus of Deformation of Concrete at Different Rates of Loading," Int. Symp., Testing In-Situ of Concrete Structures, Budapest, 1977, pp. 109 – 117.

30. Takeda, J. and Tachikawa, H., "Deformation and Fracture of Concrete Subjected to Dynamic Load," Mechanical Behavior of Materials, Proceedings of the International Conf., Vol. IV, Kyoto, 1971.

31. John, R., Antoun, T., and Rajendran, A. M., "Effect of Strain and Size on Tensile Strength of Concrete," 1991 APS Topical Conf. on Shock Compression of Condensed Matter, Williamsburg, VA, Schmidt, Dick, Forbes, and Tasker, editors, Esevier Science Publ. 1992, pp. 501 – 504.

32. Antoun, T. H., Constitutive/Failure Model for the Static and Dynamic Behaviors of Concrete Incorporating Effects of Damage and Anistropy, PhD Dissertation, The University of Dayton, Dayton, OH, 1991, p. 230.

33. McVay, M. K., "Spall Damage of Concrete Structures," Tech. Rept. SL-88-22 US Army Corps of Engineers, WES, Vicksburg, MS, 1988.

34. Malvern, L. E., Jenkins, D. A., and Dehoff, "Rate and Confinement Effects on Cracking and Failure in Uniaxial Compressive of Concrete," AFOSR-93-0071 (AD-A261 164) AF Office of Scientific Research, AFOSR/NA, Bldg. 410, Bolling AFB, DC, November 1992.

35. Ross, C. A., "Crack Patterns Resulting from High Strain Rate Tests on Concrete," ESL-TR-92-08, AF Engineering and Services Center, Tyndall AFB, FL, March 1992.

36. Tedesco, J. W., Ross, C. A., and Kuennen, S. T., "Experimental and Numerical Analysis of High Strain Rate Splitting Tensile Tests," ACI Materials Journal, Vol. 90, No. 2, March – April 1993, pp. 162 – 169.

37. Tang, T., Ouyang, C., and Shah, S. P., "Simple Method for Determining Material Fracture Parameters from Peak Loads," ACI Materials Journal, Vol. 93, No. 2, March – April 1996, pp. 147 – 157.

38. Shah, S. P., Swartz, S. E., and Ouyang, C., Fracture Mechanics of Concrete, J. Wiley & Sons, Inc., NY, 1995.